SOLID-STATE NMR STUDIES OF LUNG SURFACTANT PROTEIN-B FRAGMENTS IN MODEL AND NATURAL LUNG SURFACTANT LIPID BILAYERS

DHARAMARAJU PALLEBOINA

Solid-State NMR Studies of Lung Surfactant Protein-B Fragments in Model and Natural Lung Surfactant Lipid Bilayers

by

© **Dharamaraju Palleboina**

A thesis submitted to the
School of Graduate Studies
in partial fulfillment of the requirements for the degree of

Master of Science

Department of Physics and Physical Oceanography
Memorial University of Newfoundland

June 19th, 2012

St. John's Newfoundland, Canada

ABSTRACT

Lung surfactant, a membranous lipid-protein complex, prevents lung collapse by lowering the surface tension at the alveolar air-water interface. Surfactant protein B (SP-B) is an essential component of lung surfactant and is indispensable for life. Mini-B is a two-helix fragment of SP-B that retains significant biological activity compared to the full-length SP-B. Solid-state ^{2}H-NMR and ^{31}P-NMR were used to characterize the lipid interactions of Mini-B or the combination of the SP-B C-terminal and N-terminal fragments (SP-B_{CTERM} + SP-B_{NTERM}) in mechanically oriented and multilamellar vesicle (MLV) lipid bilayers. These were composed of a model surfactant system, POPC-d_{31} /POPG (7:3) or a natural surfactant system, DPPC-d_{62}-doped Bovine Lipid Extract Surfactant (BLES). Our results show that Mini-B or SP-B_{CTERM} + SP-B_{NTERM} tends to disrupt the bilayer structure and induce the formation of a non-oriented fraction in oriented lipid bilayers on large-scales. Mini-B had a greater effect on oriented bilayers of POPC-d_{31}/POPG than did SP-B_{CTERM} + SP-B_{NTERM}. On the other hand, SP-B_{CTERM} + SP-B_{NTERM} showed more effect on oriented bilayers of BLES than did Mini-B. Neither peptide system significantly changed lipid orientational order in POPC-d_{31}/POPG, whereas the combination of SP-B_{CTERM} + SP-B_{NTERM} did induce some ordering in the oriented fraction of BLES. The interactions of these peptide systems with MLVs were studied in order to separate effects on chain order from large length scale perturbations of bilayer orientation. Neither peptide system induced formation of rapidly tumbling structures in POPC-d_{31}/POPG vesicles whereas both did, to a small extent, in BLES vesicles. Modification of bilayer orientation in oriented lipid bilayers in presence of peptide may be relevant to the transfer of material from bilayer reservoirs to a flat surface active layer, a process that likely requires contact facilitated by the formation of highly curved protrusions. Despite its significant biophysical activity compared to full-length SP-B, Mini-B was not found to enable the formation of tubular myelin, a structure thought to be a precursor to the surface-active layer at the air-water interface.

ACKNOWLEDGEMENTS

I wish to express my foremost and sincere thanks to my supervisors Professor Dr. Valerie Booth and Professor Dr. Michael Morrow for their guidance and encouragement during the research and supervision of this thesis. This thesis would not have been finished without their financial support and motivation. I am deeply indebted to them for their great concern about my future and their generosity and patience. I am again thankful to Michael Morrow for teaching me fundamentals of NMR and working with NMR instrument and thankful to Valerie Booth for teaching me research ethics, a course "How to Become a Scientist". It is my fortune to have them my supervisors.

I would like thank my advisory committee member Professor Dr. Kaushik Nag for his valuable suggestions and encouragement during the program.

I specially thank Donna Jackman for her great help and support in assisting me how to prepare samples and working in lab in all stages of my work. I would also thank Dr. Celine Schneider for teaching me how to work with and running NMR instrument.

I warmly thank my colleges Dr. Muzaddid Sarker, James Pius, Mahzad Sharifahmadian, Nathan Andrew and Dr. Mark McDonald for their useful discussions many times during the program and it was a good time working with them in lab.

I acknowledge the support of department, staff, fellow graduate students and my other friends who contributed in one way or another toward this work or my stay in St. Johns.

At last, I wish to express my love and gratitude to my parents, my wife, and my brothers for their love, encouragement and financial support.

Table of Contents

List of Tables

List of Figures

List of Abbreviations

ARDS, Acute Respiratory Distress Syndrome

BLES, Bovine Lipid Extract Surfactant

C-D, Carbon-Deuterium

$CHCl_3$/MeOH, Chloroform/Methanol

DLS, Dynamic Light Scattering

DSC, Differential Scanning Calorimetry

DPPC, 1,2-Dipalmitoyl-*sn*-glycerol-3-phosphocholine

DPPC-d_{62}, 1,2-perdeuterodipalmitoyl-*sn*-glycerol-3-phosphocholine

EFG, Electric Field Gradient

FID, Free Induction Decay

HPLC, High-performance liquid chromatography

LC, lysophosphatidylcholine

LS, Lung Surfactant

MLVs, Multi Lamellar Vesicles

NMR, Nuclear Magnetic Resonance

NRDS, Neonatal Respiratory Distress Syndrome

PC, Phosphatidylcholine

PE, Phosphatidylserine

PG, Phosphatidylglycerol

PI, Phosphatidylinositol

PS, Phosphatidylserine

POPC, 1-palmitoyl-2-oleoyl-*sn*-glycero-3-phosphocholine

POPC-d_{31}, 1-perdeuteropalmitoyl-2-oleoyl-*sn*-glycero-3-phosphocholine

POPG, 1-palmitoyl-2-oleoyl-*sn*-glycero-3 phospho-(1'-*rac*-glycerol)

RDS, Respiratory Distress Syndrome

SPs, Surfactant proteins

SP-A, Surfactant protein A

SP-B, Surfactant protein B

SP-C, Surfactant protein C

SP-D, Surfactant protein D

S_{CD}, C-D order parameter

SM, Sphingomyelin

TEM, Transmission Electron Microscopy

TM, Tubular myelin

^{2}H-NMR, Deuterium Nuclear Magnetic Resonance

^{31}P-NMR, Phosphorous Nuclear Magnetic Resonance

Chapter 1

Lung Surfactant

1.1 Lung surfactant counteracts surface tension in lung

Breathing is an essential function for life that happens automatically for humans and other mammals. Breathing couldn't happen without the lungs of the respiratory system where oxygen and carbon dioxide are passively exchanged by diffusion between the alveolar regions of the lungs and external environment (air). In lungs, there are about 300 million alveoli, each of which is 75-300 μm in diameter, which means lungs have a surface area of 140 m^2 in contact with air when maximally expanded (Notter 2000). Exposure of such a large alveolar surface area is required for adequate gas exchange in lungs.

Because lung function requires contact with the environment at atmospheric pressure in the alveoli, the inner surface area of the alveoli coated by aqueous layer gets dry up due to increasing surface tension, which results in lung collapse. Lung collapse must be prevented by reducing surface tension at the alveolar air-water interface (Possmayer 1997). This is accomplished by a material called lung surfactant (LS), which prevents lung collapse at the end of expiration and eases the work of breathing during the subsequent breathing cycles. Lung surfactant is also called pulmonary surfactant. Lung surfactant function starts during the first breath and continues throughout life.

In lung surfactant, the surface active-material is a membranous lipid-protein complex whose main function is to reduce surface tension at the alveolar air-liquid interface of lungs (Pattle 1995, Clements 1957). Lung surfactant contains mostly phospholipids, which are amphipathic in nature - they have both water-loving (hydrophilic) and water-hating (hydrophobic) regions. They orient with their head groups in contact with the alveolar liquid layer and their acyl chains in contact with the air at the air-liquid interface. Since the surface tension arises from the attractive forces of liquid molecules, binding of phospholipid molecules with liquid will tend to counteract this attraction and consequently reduce the surface tension of liquid lining the alveoli. This reduces the pressure required to maintain the air space in the alveolus according to

Laplace's Law $P = \frac{2\gamma}{r}$ where P is the of the enclosed gas pressure, γ is the surface tension and r is the radius of an alveolus (Clements 1957).

1.2 Lung surfactant composition

Lung surfactant is a complex mixture of lipids and proteins. Lung surfactant obtained from bronchoalveolar lavages of human lungs contains 80% phospholipids (by weight), 10% neutral lipids and 10% proteins (Veldhuizen et al. 1998). The phospholipid fraction of lung surfactant consists mostly of phosphatidylcholine (PC). Among the phospholipid fraction, 40% is dipalmitoyl phosphatidylcholine (DPPC), 20% is unsaturated PC, 10% is phosphatidylglycerol (PG) while the remaining 10 % consists of phosphatidylinositol (PI), phosphatidylethanolamine (PE), phosphatidylserine (PS), lysophosphatidylcholine (LC) and sphingomyelin (SM). There are some cases where DPPC content is as low as 15% for some hetero thermal mammals (which have a body temperature that changes with environment) (Lang et al. 2005). In general, for adults PG levels are higher than PI, whereas for fetal lungs PI is higher than PG. The neutral lipid fraction consists mainly of cholesterol, small amounts of monoacyl glycerol, diacyl glycerol, triacyl glycerol and free fatty acids, mainly palmitate. There are four surfactant proteins that have been identified so far. They are SP-A, SP-B, SP-C and SP-D, according to their chronological order of discovery (King et al. 1973, Johansson et al. 1994). The composition of surfactant can vary with age and is also influenced by diet and physical fitness (Crewels 1997).

Alveolar cells, called type II pneumocytes, synthesize both lipids and proteins in lung surfactant (Wright and Clements 1989). These type II cells secrete surfactant into alveoli in the form of lamellar bodies, a densely packed concentric multilamellar structure. The process by which the surfactant material in lamellar bodies is incorporated into the surface active film at the air-water interface remains poorly understood. Tubular myelin, a highly organized protein-lipid structure which appears to be an array of bilayer tubules, has been observed in electron micrographs of lung surfactant lavage, leading to

suggestions that it might play an intermediate role in formation of the surface active film (Orgeig et al. 2004, Lumb 1989). However, the viability of mutants that lack the capacity to form tubular myelin suggests it may not be essential for lung function (Ikegami 1998).

1.3 Lung surfactant proteins

As stated above, surfactant proteins together make up 10% of the weight of surfactant. The characteristics of lung surfactant proteins (SPs) are listed below (see Table 1.1).

Table 1.1 Characteristics of four lung surfactant proteins (Serrano and Perez-Gil 2006, Zuo et al. 2008)

Surfactant protein	Number of amino acids	Molecular weight (kDa)	Quaternary Structure	Polarity	Homologues
SP-A	248	26-38	Octodecamer	Hydrophilic	Collectins
SP-B	79	8.7	Dimer	Hydrophobic	Saposins
SP-C	35	4.2	Monomer	Hydrophobic	--
SP-D	355	43	Dodecamer	Hydrophilic	Collectins

SP-A and SP-D are hydrophilic surfactant proteins, which dissolve in polar solvents and are negatively charged at physiological pH. They belong to the collectin family of collagenous carbohydrate-binding proteins (Crewels 1997). These collectin family proteins contain groups of collagen-like domains and lectin domains. SP-A is the most abundant protein among all lung surfactant proteins, comprising 5-6% (dry weight) of surfactant. SP-A plays critical roles in the function of lung surfactant including 1) the association of SP-A with lipid in the formation of tubular myelin (TM) with calcium (Ca^{2+}), 2) host defense through the binding of bacteria and viruses, and 3) acceleration of the insertion and replenishment of surfactant film material at the air-liquid interface during breathing cycles (Crewels 1997). SP-D is the largest of all lung surfactant proteins. Like SP-A, SP-D also plays a primary role in host defense.

SP-B and SP-C are hydrophobic proteins that dissolve in non-polar solvents, are positively charged at physiological pH, and are smaller than the two hydrophilic proteins SP-A and SP-D (Table 1.1) (Perez-Gil 1993). Both of these hydrophobic surfactant proteins have been implicated in a number of biophysical processes in the lung surfactant system. They have similar roles in enhancing the adsorption and reorganization of surfactant monolayer components at the air-water interface of alveoli during subsequent breathing cycles (Johansson et al. 1994). These two proteins may facilitate the exclusion of some surfactant components from the monolayer and their reinclusion back to the monolayer during expansion of the lungs (Perez-Gil 2008). Similar to SP-A, SP-B also plays a critical role in the formation of TM in the presence of calcium (Ca^{2+}). Dysfunction of SP-B leads to incomplete processing of SP-C protein (Rooney 1998). These hydrophobic membrane proteins interact with membrane bilayers and it is proposed that SP-B is bound to the membrane surface (as a peripheral membrane protein) whereas SP-C is buried within the membrane bilayer (as an integral membrane protein).

1.4 Function and biophysical activity

The activity of surfactant can be divided into mainly three processes: 1) transfer of surface-active molecules from hypophase (the liquid layer) into the air-liquid interface; 2) reduction of the surface tension to minimum values ($\approx$ 0 mN/m) during compression; 3) respreading of surfactant components during expansion. DPPC alone is capable of reducing the surface tension to lower values (Nag et al. 1999, Cruz et al. 2000), but it cannot adsorb and re-spread quickly enough during the breathing cycles. On the other hand, unsaturated PG and PC are fluid enough for fast spreading but cannot alone lower the surface tension sufficiently at physiological conditions (Takamoto 2001). So, the above individual components are individually good at lowering the surface tension or promoting fast re-spreading, but none of them individually exhibit both properties at physiological conditions. The gel-liquid crystalline transition temperature (transition to the liquid crystalline phase above this temperature) of pure DPPC bilayers is 41^{o}C, which is above the physiological temperature. Below the transition temperature, DPPC lipid bilayers are in the gel phase. The gel-liquid crystalline transition temperatures of bilayers

of unsaturated palmitoyl-oleoyl-phosphatidylcholine (POPC) or palmitoyl-oleoyl-phosphatidylglycerol (POPG) are -2 °C, far below the physiological temperature. So, the presence of a significant amount of unsaturated phospholipids, in addition to DPPC, is required to reduce the transition temperature of surfactant bilayers to below the physiological temperature of 37 °C (Perez-Gil 2008). Thus, lung surfactant needs to be a mixture of different types of lipids and proteins.

Pattle proposed what is known as the classical model for lung surfactant function. According to this model, lungs contain DPPC, PC and PG (Pattle 1955). The monolayer at the air-liquid interface of the alveolar surface is covered with pure DPPC which lowers surface tension to minimum values under compression during expiration. The squeeze-out hypothesis proposed by Clements suggests that lateral compression of mixed phospholipids in the monolayer during compression results in the loss of the least stable components, such as the fluid unsaturated PC and PG constituents, thereby generating a monolayer composed of the most stable component, DPPC, at the end of expiration (Pastrana-Rios 1994). This hypothesis ruled the lung surfactant world for nearly 30 years.

More recently, the squeeze-out hypothesis has been updated to include surfactant reservoirs which are located right below the monolayer at the air-liquid interface. The surfactant proteins link the surface monolayers with the surfactant reservoirs. Squeeze-out components during compression would temporarily reside in surfactant reservoirs right below the air-liquid interface (Schurch et al. 1995). The components within the reservoirs would release and re-spread along the air liquid interface during inspiration. This would allow unstable phospholipids to leave monolayers during compression and restore the surfactant films during expansions of respiratory cycles.

1.5 Surfactant deficiency or dysfunction

Inactivation of a surfactant system due to surfactant deficiency or dysfunction causes respiratory distress syndrome (RDS) (Lynch 2004). RDS is classified into two types: 1) Neonatal Respiratory Distress Syndrome (NRDS), which can affect premature

infants born before they produce sufficient amounts of surfactant; and 2) Acute Respiratory Distress Syndrome (ARDS), a lung disease in adults due to surfactant dysfunction caused by illness or injury. Surfactant replacement therapy for infants improved the rate of mortality greatly for NRDS, but surfactant therapy for ARDS has not been shown to improve mortality rates and research is ongoing (Wiedemann and Tai 1997, Gunther et al. 2001).

1.6 Lung Surfactant Protein B (SP-B)

Lung surfactant protein SP-B is essential, i.e. human or model animals born without SP-B do not survive. Human SP-B is a 79 residue protein with the following sequence (Hawgood et al. 1998).

Phe^{1}-Pro^{2}-Ile^{3}-Pro^{4}-Leu^{5}-Pro^{6}-Tyr^{7}-Cys^{8}-Trp^{9}-Leu^{10}-Cys^{11}-Arg^{12}-Ala^{13}-Leu^{14}-Ile^{15}-Lys^{16}-Arg^{17}-Ile^{18}-Gln^{19}-Ala^{20}-Met^{21}-Ile^{22}-Pro^{23}-Lys^{24}-Gly^{25}-Ala^{26}-Leu^{27}-Ala^{28}-Val^{29}-Ala^{30}-Val^{31}-Ala^{32}-Gln^{33}-Val^{34}-Cys^{35}-Arg^{36}-Val^{37}-Val^{38}-Pro^{39}-leu^{40}-Val^{41}-Ala^{42}-Gly^{43}-Gly^{44}-Ile^{45}-Cys^{46}-Gln^{47}-Cys^{48}-Leu^{49}-Ala^{50}-Glu^{51}-Arg^{52}-Tyr^{53}-Ser^{54}-Val^{55}-Ile^{56}-Leu^{57}-Leu^{58}-Asp^{59}-Thr^{60}-Leu^{61}-Leu^{62}-Gly^{63}-Arg^{64}-Met^{65}-Leu^{66}-Pro^{67}-Gln^{68}-Leu^{69}-Val^{70}-Cys^{71}-Arg^{72}-Leu^{73}-Val^{74}-Leu^{75}-Arg^{76}-Cys^{77}-Ser^{78}-Met^{79}.

SP-B is synthesized as a longer precursor of 381 amino acids; it then undergoes proteolytic cleavage of N- and C- terminal propeptides to form a mature SP-B which consists of residues 201-279 of the main precursor. SP-B processing then continues in three discrete steps to form the final version of SP-B (Hawgood et al. 1998).

SP-B is a disulphide-linked homodimer of approximately 18 kDa. Each monomer of SP-B contains seven cysteines, of which six form three intramonomer disulphide bonds linking Cys 8↔Cys77, Cys 11↔Cys 71 and Cys 35↔Cys 46. The seventh cysteine, at position 48, forms an intermolecular bridge between two monomers that

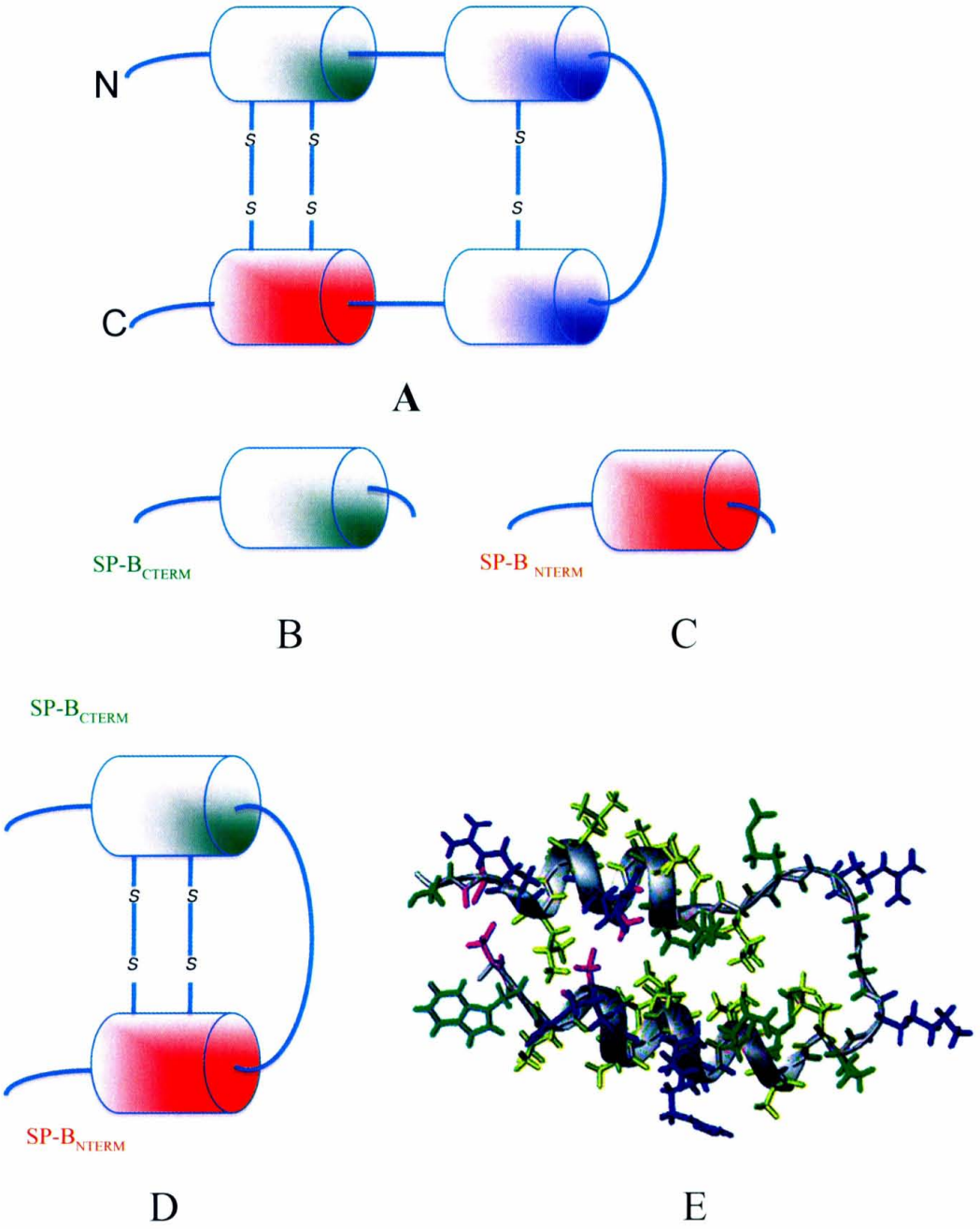

Figure 1.1. Schematic representations of A) full length SP-B, B) SP-B_{CTERM}, C) SP-B_{NTERM}, and D) Mini-B. The structure of Mini-B in SDS micelles is shown in (E). Reprinted with permission from "*Sarker M, Waring AJ, Walther FJ, Keough KM, Booth V (2007). Structure of Mini-B, a functional fragment of surfactant protein B, in detergent micelles. Biochemistry; 46, 11047-11056*". *Copyright "2007" American Chemical Society.*

stabilize the dimeric from of SP-B. Human SP-B has nine positively and two negatively charged amino acids which give a net charge of +7 per subunit at neutral pH. SP-B sequence alignment and the location of the cysteine residues show that SP-B belongs to the saposin super family (Hawkins et al. 2005, Liepinsh et al. 1997). All saposin family proteins share a similar secondary structure. Thus SP-B is expected to contain four to five amphiphilic helices. The three-dimensional structure of full length SP-B is not yet known, but high-resolution structures of fragments of SP-B are available (Booth et al. 2004; Sarker et al. 2007, Kurutz and Lee 2002).

Studies of SP-B in lipid bilayers using Fourier Transform Infrared Spectroscopy (FTIR) suggest that SP-B orients with its helices parallel to the lipid bilayer such that hydrophobic residues of the protein are buried inside the hydrophobic core of the bilayer and charged residues interact with phospholipid head group (Vandenbusshe et al. 1992). It was proposed that due to its cationic nature (+7) SP-B specifically interacts with anionic phospholipids, PGs (Perez-Gil 1995).

Synthetic fragments of SP-B have been found to show similar functional properties to those of native SP-B in some animal models. The synthetic fragments of SP-B are SP-B_{CTERM}, SP-B_{NTERM}, Mini-B and super Mini-B. Studies of surfactant-deficient rats treated with fragments of SP-B suggest that Mini-B performs as well or better than SP-B, that SP-B_{CTERM} has about one third the biological activity of SP-B and SP-B_{NTERM} has almost no activity at all (Waring et al. 2005).

SP-B_{CTERM} (SP-B_{63-78}) comprises 16 amino acids residues from positions 63-78 of full length SP-B and encompasses the C-terminal helix. SP-B_{NTERM} (SP-B_{8-25}) comprises 18 amino acid residues from positions 8-25 of full length SP-B and encompasses the N-terminal helix. Mini-B is a 34-residue peptide constructed with the combination of both SP-B_{CTERM} and SP-B_{NTERM} helices connected by a loop and two disulfide bonds. Super Mini-B is Mini-B but with an extra amino acid sequence (1-7) of native SP-B inserted at N-terminal end of Mini-B.

1.7 Why Mini-B is important

Mini-B has the following similarities to SP-B:

1. In *in vivo* studies, surfactant-lavaged rats treated with Mini-B showed better oxygenation and dynamic compliance in comparison to SP-B itself (Waring et al. 2005, Walther et al. 2010);
2. Mini-B contains two disulphide bonds at the same positions as in native SP-B, Cys 8↔Cys77 and Cys 11↔Cys 71;
3. Mini-B has a net charge of +7 similar to SP-B;
4. Like SP-B, Mini-B is also amphipathic in nature with a large hydrophobic face one side and a hydrophilic face on other side.

1.8 SP-B-lipid interactions

SP-B plays a vital role in the function of lung surfactant. Functional roles that have been suggested for SP-B include membrane binding, membrane lysis and membrane fusion (Hawgood et al. 1998). It plays a critical role in rapidly inserting phospholipids into the surface-active layer and hence in the formation of the surface-active layer at the air-water interface. It is suggested that SP-B induces lipid exchange by holding surfactant reservoirs in close contact with the interfacial monolayer thereby promoting monolayer-bilayer contacts (Cruz et al. 2000). In this way SP-B could keep sqeezed-out components in surfactant reservoirs during compression. Recent simulations (Baoukina and Tieleman 2011) also suggested that SP-B promotes transfer of lipid between bilayer reservoirs and monolayer. It is thought to interact preferentially with the PG fraction of lipid due to the electrostatic interaction between positively charged residues of SP-B and negatively charged phospholipid headgroups (Baat et al. 1990).

SP-B strongly interacts with surfactant lipid and promotes lipid packing perturbations in both membrane bilayers and monolayers (Serrano and Perez-Gil 2006). In spite of the critical role of SP-B in lung surfactant function, the complex mechanisms

involved in the interactions of SP-B with lipids are still not well understood. Solid-state NMR, Differential Scanning Calorimetry (DSC), Dynamic Light Scattering (DLS), Infrared Spectroscopy (IR Spectroscopy) and Transmission Electron Microscopy (TEM) have been used to study the interactions of lipid and proteins in bilayers. Solid-state NMR is one of the most versatile techniques used to study the interactions of SP-B with lipids in the bilayer. Previous ^{2}H-NMR studies of chain and headgroup labeled phospholipids in multilamellar vesicle surfactant model systems have shown small perturbations of lipid chain orientational order, and thus lipid area, resulting from interactions with SP-B and its fragments (Dico et al. 1997, Russell-Schulz et al. 2009).

A recent study of SP- B_{CTERM} in mechanically oriented bilayers of POPC, POPG, POPC/POPG, and bovine lipid extract surfactant (BLES) showed that SP-B_{CTERM} perturbed oriented lipid bilayer structure of lipid bilayer and changed the orientational order of acyl chain in lipid bilayers (Yang et al. 2009). These perturbations are probably relevant to the function of SP-B in lung surfactant system.

1.9 Tubular Myelin

Tubular myelin (TM) is thought to be an intermediate step in the sequence of structural changes that takes place in the pathway of lung surfactant forming a monolayer at the air-water interface. Lung surfactant proteins (SP-B and SP-A) and lipid (DPPC and egg PG) plays a important role in the formation of TM. The structure of tubular myelin looks like square lattices and elongated tubules. However, the mechanism by which the proteins and lipids promote TM structure are not well understood. A potential mechanism for conversion of lamellar bodes into tubular myelin was presented by Willams (Williams 1977). His observations suggest the continuity between lamellar body and tubular myelin. High-resolution immunoelectron microscopy (Voorhout et al. 1991) suggests that SP-B plays a vital role in the formation of tubular myelin by fusion of bilayers in presence of SP-A and calcium where SP-A appear to locate at junctions of TM lattices and each side of the lattice is about 40-50 nm.

1.10 Objectives of present work

SP-B is the most essential component in lung surfactant (Clark et al. 1995). It plays a vital role in maintaining the surfactant and facilitating lipid transfer between the monolayer and the bilayer reservoirs (Parez-Gil 2002). The mechanism by which SP-B interacts with lipids in the lung surfactant system is not known. *In vivo* studies suggest that fragments of SP-B, Mini-B, SP-B_{CTERM} and SP-B_{NTERM} retain significant biological activity in comparison to SP-B. Understanding the interactions of these fragments of SP-B with lipids in lipid bilayers will provide insights into the function role of SP-B and may also be useful in development of synthetic lung surfactant peptides.

The present study is focused on how SP-B_{CTERM} and SP-B_{NTERM}, either linked in the form of Mini-B or together but unlinked, interact with lipids in the lipid bilayer system composed of a model lung surfactant mixture POPC/POPG (7:3) and a natural lung surfactant mixture Bovine Lipid Extract of Surfactant (BLES). Here we employed two types of model bilayer systems, oriented bilayers and multilamellar vesicle bilayers. This study provides useful formation about how these SP-B fragments, in the form of Mini-B or together but unlinked, perturb bilayer systems and how such effects depend on lipid composition. In order to get insights into these questions, ^{2}H and ^{31}P solid-state NMR were employed to study these lipid-protein interactions. Comparing perturbation of mechanically-oriented bilayers and multilamellar vesicles by Mini-B or the component helices SP-B_{CTERM} and SP-B_{NTERM} provides some evidence that these peptides might promote the formation of protrusions that could facilitate close bilayer-monolayer contact as expected in some models of reservoir formation, maintenance, and re-adsorption.

The hydrophobic protein SP-B plays a critical role in the formation of tubular myelin, which is believed to be a precursor of surface active film at the air-water interface (Parez-Gil and Weaver 2010). As Mini-B shows significant biological activity, we would also like to know if Mini-B can enable formation of tubular myelin. The results of such a study could tell us whether the formation of tubular myelin is important for the function of lung surfactant.

Chapter 2

Solid-state NMR

Solid-state nuclear magnetic resonance, especially deuterium nuclear magnetic resonance (^{2}H-NMR), is an important way to study the effect of membrane proteins on lipid bilayer properties (Davis 1983). In particular, it provides useful information about structure and dynamics of model and biological membranes. In order to use ^{2}H-NMR, hydrogen atoms, typically on all or part of the chains, are replaced by deuterium atoms. Replacement of hydrogen by deuterium is called deuterium labeling. This does not alter the physical properties and molecular structure of the system to be studied. ^{2}H-NMR is thus a non-perturbing probe technique.

2.1 Deuterium-NMR

The total Hamiltonian of a deuterium nucleus in the presence of an external magnetic field B_0 is given by

$$H = H_0 + H_Q + H_{CS} + H_D \qquad \text{..... (1)}$$

where H_0 is the Zeeman interaction with the external magnetic field, H_Q is the quadrupolar interaction that arises from interaction of the nuclear magnetic moment with the electric field gradient of a carbon-deuterium bond, H_{CS} is the anisotropic chemical shift interaction due to shielding by electron density around the deuterium nucleus and H_D is the dipolar coupling that arises from the interaction between two magnetic dipole moments. The magnitudes of these interactions can be compared by considering the extent to which they perturb the deuteron NMR frequency. In comparison to the quadrupolar coupling, the chemical shift for deuterium is very small and less than 1 kHz and the dipolar interaction between two deuterium nuclei is approximately 4 kHz. The dipolar and chemical shift interactions thus are negligible when compared to the quadrupolar splitting of 250 kHz for deuterium in a static C-^{2}H bond. Therefore, one can write the total Zeeman interaction and the quadrupole interaction as

$$H \approx H_0 + H_Q. \qquad \text{..... (2)}$$

The deuterium nucleus possesses spin=1 (one proton and one neutron). Its natural abundance is 0.016%. In the presence of an external magnetic field, it has three energy levels corresponding to the azimuthal quantum numbers m=1, 0, -1. A nucleus with spin≥1 has a non-spherical charge distribution, and thus an electric quadruple moment. Due to this non-spherical nuclear charge distribution there is an electrostatic interaction between the nuclear quadrupolar moment and the electric field gradient (EFG) at the position of the nucleus. This quadrupolar interaction perturbs the Zeeman energy levels such that the degeneracy between the two transitions is removed which results in two allowed transitions as shown in Figure 2.1.

The following treatment is based on descriptions presented by Davis (1983) and Seelig (1977). The expression for the total energy can be written as

$$E_m = -gm\beta_N H_0 + \frac{e^2qQ}{4I(2I-1)}[3m^2 - I(I+1)]\left[\left(\frac{3\cos^2\beta' - 1}{2}\right) + \frac{1}{2}\eta\sin^2\alpha\cos 2\beta'\right], \quad \text{..... (3)}$$

where β, α indicates the orientation of the EFG tensor with respect to the external magnetic field B_0, g is g-factor of the nucleus and η is the asymmetry parameter which reflects departures of the electric field gradient from axial symmetry. The selection rule allows $\Delta m = \pm 1$ (-1 $\rightarrow$ 0 and 0 $\rightarrow$ +1). The transition frequency can be related to the difference between energy levels by $\Delta E = h\nu$.

The resonance frequencies that corresponds to the allowed transitions are

$$\nu_- = \frac{\gamma H_0}{2\pi} + \frac{3e^2qQ}{4h}\left[\left(\frac{3\cos^2\beta' - 1}{2}\right) + \frac{1}{2}\eta\sin^2\alpha\cos 2\beta'\right] \quad \text{..... (4)}$$

and

$$\nu_+ = \frac{\gamma H_0}{2\pi} - \frac{3e^2qQ}{4h}\left[\left(\frac{3\cos^2\beta' - 1}{2}\right) + \frac{1}{2}\eta\sin^2\alpha\cos 2\beta\right]. \quad \text{..... (5)}$$

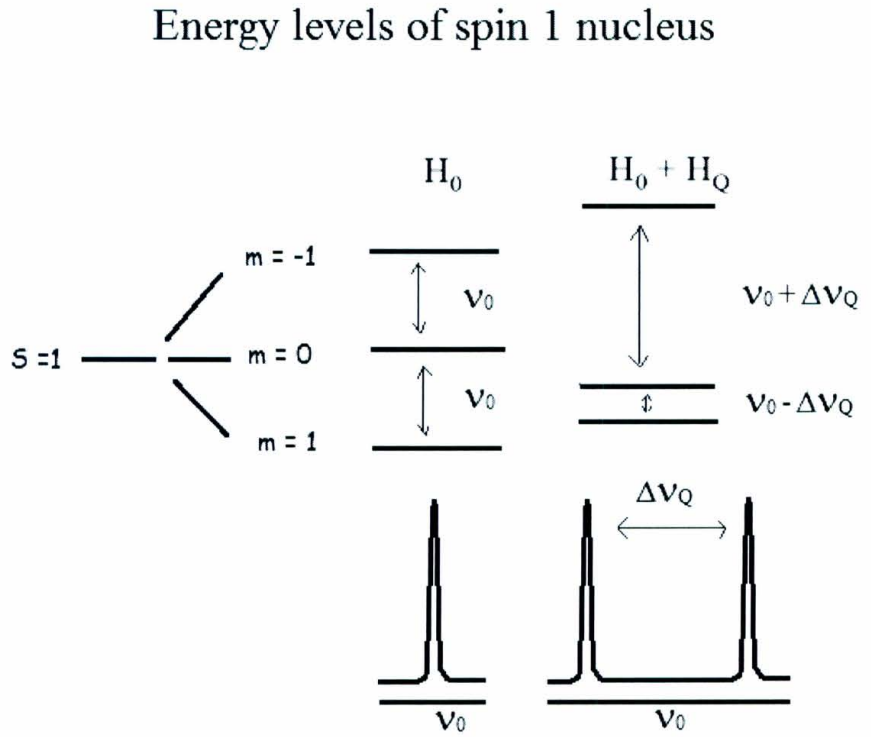

Figure 2.1: Schematic representation of the effect of the quadrupolar interaction on Zeeman energy levels of a ^{2}H nucleus. The single line at ν_0 is split by the quadrupolar interaction.

These resonance frequencies are symmetrically centered on the Larmor frequency ν_o and the separation between these two frequencies is termed the quadrupolar splitting ($\Delta\nu_Q = \nu_- - \nu_+$) and given by

$$\Delta\nu_Q = \frac{3e^2qQ}{2h}\left[\left(\frac{3\cos^2\beta' - 1}{2}\right) + \frac{1}{2}\eta\sin^2\alpha\cos 2\beta\right]. \qquad \ldots\ldots\ldots\ldots\ldots (6)$$

The term ($e^2qQ/2h$) in Equation 6 is called the quadrupolar coupling constant and is 167 kHz for C-D bonds (Burnett and Muller 1971). In the case of C-^{2}H bonds, the EFG tensor

is nearly axially symmetric about the magnetic field, so η~0. The expression in Equation 6 then reduces to

$$\Delta\nu_Q = \frac{3e^2qQ}{2h}\left(\frac{3\cos^2\beta' - 1}{2}\right). \qquad \text{..... (7)}$$

In solution NMR the quadrupolar splitting is averaged to zero due to isotropic molecular reorientations. In solid-state NMR, molecules move anisotropically and the quadrupolar splitting is not zero. Equation 7 refers to the quadrupolar splitting for static C-D bonds. This expression must be modified for liquid crystalline lipid bilayer phases where the quadrupolar interaction is partially averaged by lipid motions and reorientation.

In the liquid crystalline phase, phospholipid molecules undergo fast axially symmetric reorientations about the bilayer normal. They also undergo conformational changes resulting from rotations about carbon-carbon bonds in the lipid acyl chain. These motions partially average the quadrupolar interaction and reduce the quadrupole splitting for a given chain deuteron. Because motion in the liquid crystalline phase is axially symmetric with respect to the bilayer normal, it is convenient to define angle β as the angle between the bilayer normal and the magnetic field and angle θ as the angle between the carbon-deuterium bond and the bilayer normal. These angles are illustrated in Figure 2.2. The angle θ then varies rapidly as a result of lipid reorientation and chain conformational changes while β changes too slowly to contribute to averaging of the quadrupole interaction. The quadrupole splitting can thus be expressed as

$$\Delta\nu_Q = \frac{3e^2qQ}{2h}\left(\frac{3\cos^2\beta - 1}{2}\right)\left\langle\frac{3\cos^2\theta - 1}{2}\right\rangle \qquad \text{..... (8)}$$

or

$$\Delta\nu_Q = \frac{3e^2qQ}{2h}\left(\frac{3\cos^2\beta - 1}{2}\right)S_{CD} \qquad \text{..... (9)}$$

Where $S_{CD} = \left\langle \frac{3\cos^2\theta - 1}{2} \right\rangle$ ..... (10)

is the orientational order parameter for a carbon-deuterium bond and the average is over motions that contribute to averaging of the quadrupolar interaction.

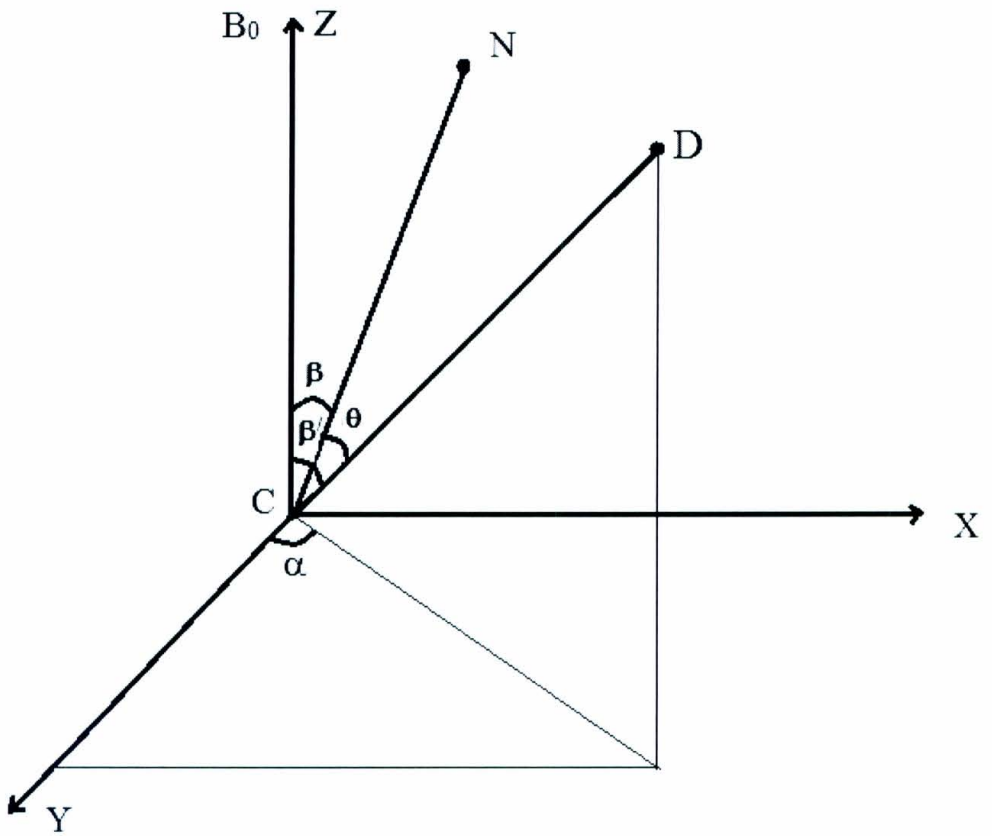

Figure 2.2: Schematic representation of the orientation of magnetic field direction B_0, bilayer normal N and C-D bond orientation relative to the principle coordinate system.

2.2 ^{2}H-NMR spectrum of a lipid chain deuterated on a single carbon

2.2.1 Oriented sample

In an oriented sample, as shown in Figure 2.3 (A), all lipids are oriented in a particular direction and there is thus a single value of β. If the lipids are deuterated only on a single chain carbon, all the deuterium nuclei in the sample are identical and thus have same S_{CD}. The spectrum is thus a single doublet as shown in Figure 2.3 (B) with a quadrupole splitting given by Equation 9 evaluated for those values of β and S_{CD}.

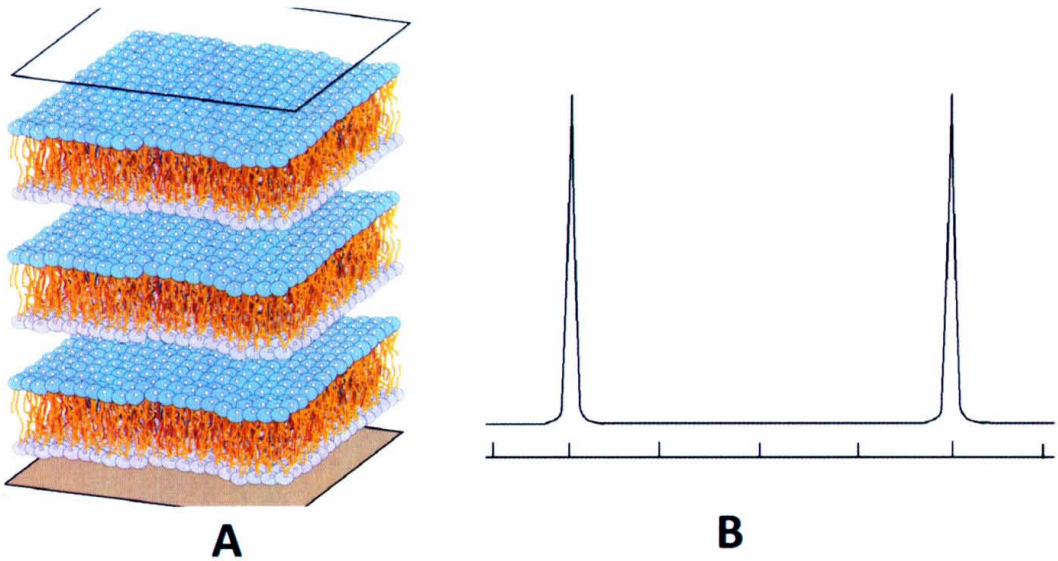

Figure 2.3: Cartoon of (A) oriented lipid bilayers, and (B) the quadrupolar split doublet for a singly-deuterated lipid chain undergoing fast axially-symmetric reorientation of the bilayer normal in an oriented lipid bilayer.

2.2.2 Powder or vesicle sample

For a polycrystalline sample or multilamellar vesicle type of sample (shown in Figure 2.4), bilayer normals are oriented with equal probability in all possible directions. β is not a constant but takes on all values from 0^o to 180^o with a weighting proportional to

the fraction of a spherical surface corresponding to that orientation. Therefore, the intensity of the deuterium spectrum varies as a function of β and the deuterium spectrum has the characteristic line shape shown in Figure 2.5.

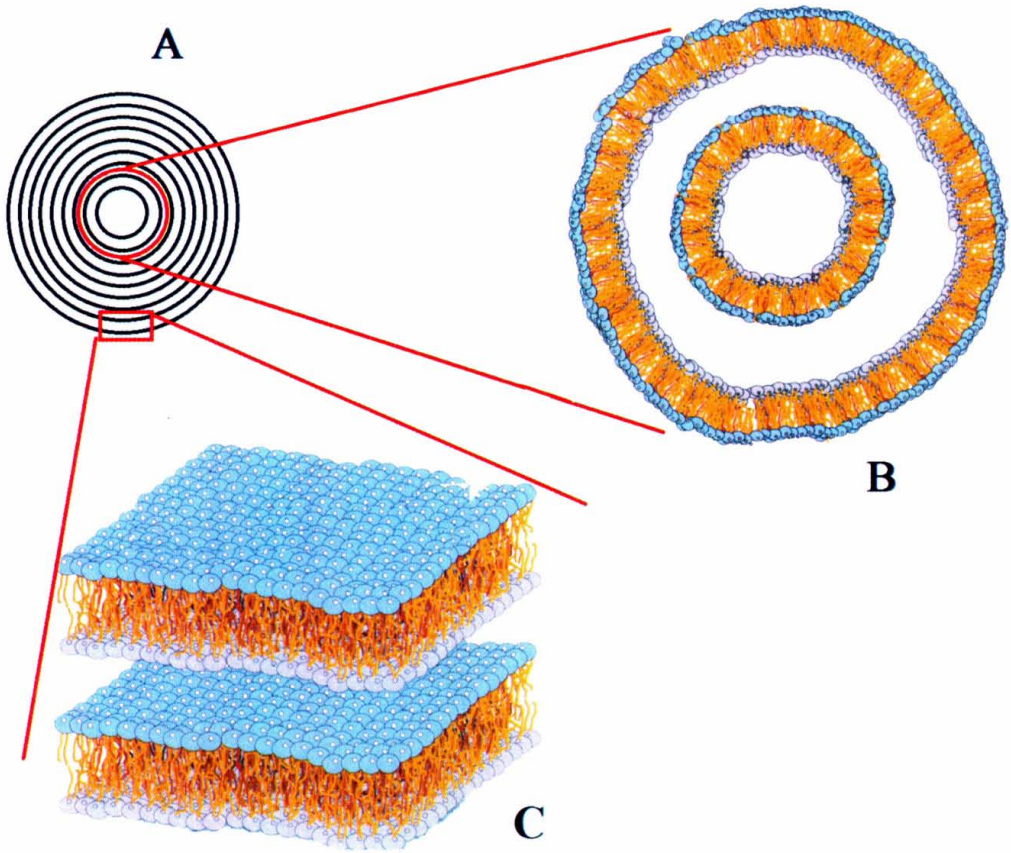

Figure 2.4: A) Schematic representation of a multilamellar vesicle. B) Individual bilayer lamellae each corresponding to a "circle" in vesicle schematic (A). C) Orientation of lipid bilayes in the small selected region of vesicle schematic (A).

The deuterium spectrum for a randomly oriented sample, shown in Figure 2.5, is a superposition of doublets from all orientations. This shape is called a Pake-doublet and is symmetric about the Larmor frequency. The dashed line in Figure 2.5 represents one of the two deuteron transitions. The highest doublet intensity is from regions of the spherical

vesicle with the bilayer normals oriented perpendicularly to the magnetic field ($\beta=90^0$) and the lowest intensity is from regions with bilayer normals oriented parallel to the magnetic field ($\beta=0^0$). The quadrupolar splitting of the prominent edges corresponding to the $\beta= 90^o$ orientation is half of the quadrupolar splitting corresponding to the $\beta=0^o$ orientation. The quadrupolar splitting ($\Delta\nu_Q$) for a powder pattern is defined as the splitting of the prominent edges corresponding to $\beta=90^o$.

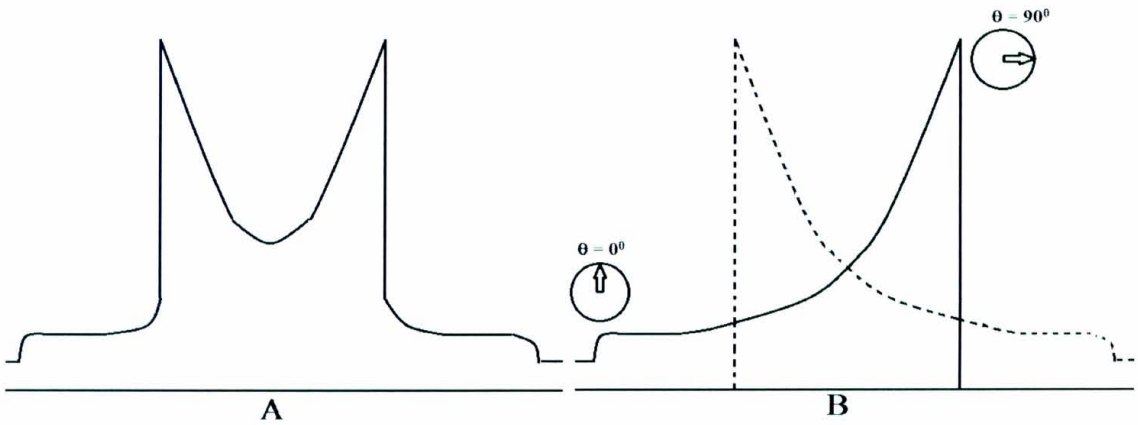

Figure 2.5: A) Cartoon of the deuterium spectra for a powder sample. B) Separation of the deuterium powder spectrum into spectral components (one solid and one dashed) corresponding to the two deuteron transitions.

2.3 ^{2}H-NMR of chain-perdeuterated lipid bilayers

The discussion so far has dealt with bilayer samples in which each lipid molecule is deuterated at a single site. The following deals with samples containing perdeuterated lipids in which all positions along the chain are deuterated. With perdeuterated lipid samples, information about the entire chain can be obtained from a single experiment.

2.3.1 Oriented sample containing chain-perdeuterated lipids

Deuterons attached to different carbons along a lipid acyl chain undergo different motions and thus have different orientational order parameters (S_{CD}). Therefore, for a particular orientation of bilayer normal in a magnetic field (oriented bilayer), the deuterium spectra is a superposition of all the doublets from deuterons along the chain.

Rewriting Equations 8 and 10 for specific positions along the lipid acyl chain gives

$$\Delta\nu_Q = \frac{3e^2qQ}{2h}\left(\frac{3\cos^2\beta - 1}{2}\right)\left\langle\frac{3\cos^2\theta_n - 1}{2}\right\rangle \qquad \text{..... (11)}$$

and

$$S_{CD}(n) = \left\langle\frac{3\cos^2\theta_n - 1}{2}\right\rangle \qquad \text{..... (12)}$$

where θ_n is the angle between C-D bond for n^{th} carbon position and the bilayer normal. Figure 2.6 illustrates the quadrupolar splittings for oriented POPC-d_{31}/POPG. Each doublet in Figure 2.6 is assigned to specific carbon positions along the saturated chain of POPC-d_{31} as shown on the left side of Figure 2.6.

The smallest quadrupolar splitting is from the methyl groups (CD_3), at the end of each chain, the motions of which are least constrained and thus result in the greatest motional averaging relative to that of other chain segments. The biggest quadrupolar splitting is from the methylene (CD_2) groups near to the head group of phospholipid, where motions are most constrained and motional averaging is small. The quadrupolar splitting thus increases from the end of the acyl chain to near to the head group due to increasingly constrained motion as shown in Figure 2.6.

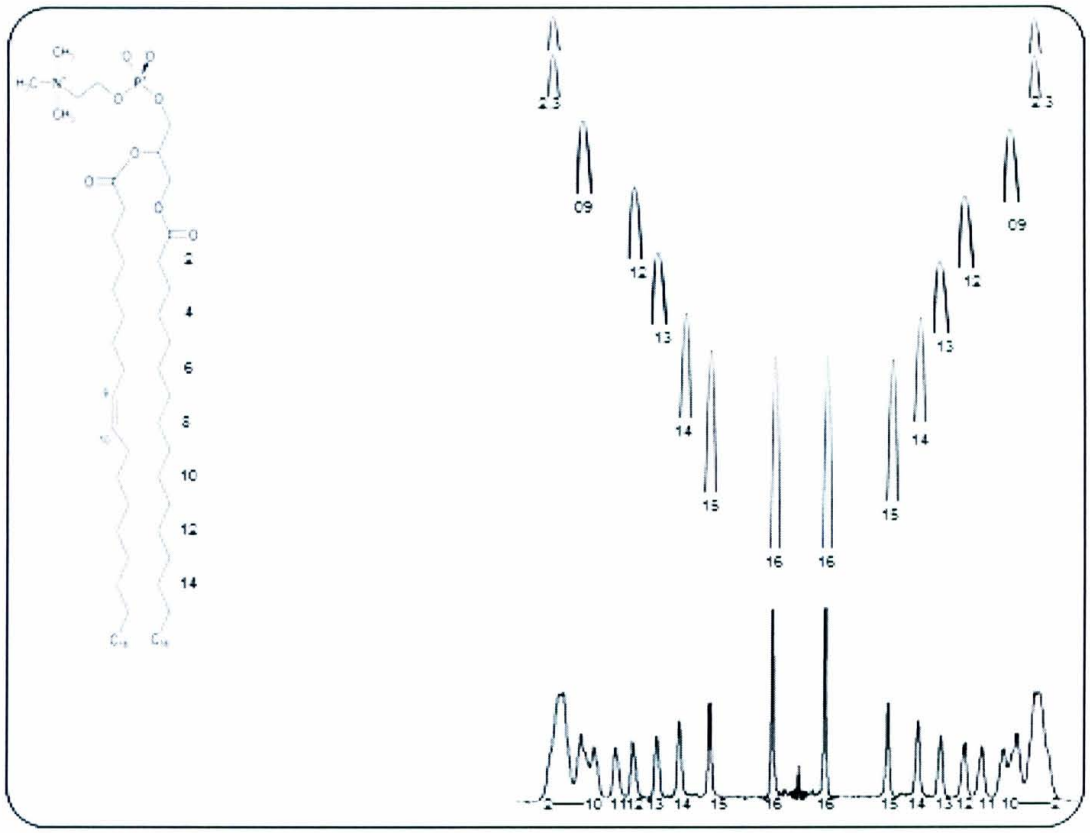

Figure 2.6: ^{2}H-NMR spectrum of oriented POPC-d_{31}/POPG lipid bilayers. Each quadrupolar splitting is assigned to a segment of the saturated phospholipid acyl chain with numbering from 2-16. The C_1 carbon does not carry a hydrogen atom and thus not deuterated.

Figure 2.7 shows that the quadrupolar splitting for a sample oriented with its bilayer normal perpendicular to the magnetic field is half of the quadrupolar splitting for a sample with its bilayer normal oriented parallel to the magnetic field. The presence of an unoriented bilayer fraction resulting from the addition of peptide or protein to oriented bilayers should thus be easily observable in orientated deuterium-NMR spectrum of a sample of mechanically oriented bilayers.

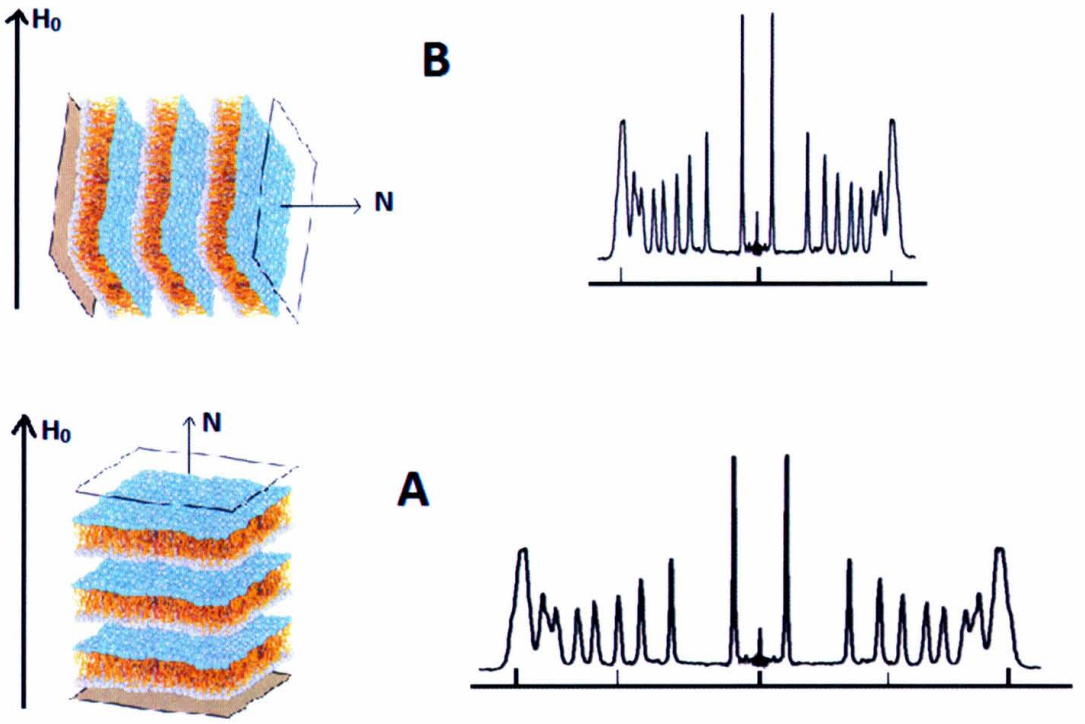

Figure 2.7: The ^{2}H-NMR spectra for oriented samples with A) bilayer normals parallel to external magnetic field, and B) bilayer normals perpendicular to external magnetic field.

2.3.2 Multilamellar vesicle samples containing chain perdeuterated lipid

The ^{2}H-NMR spectrum of a multilamellar vesicle sample containing chain perdeuterated lipid is a superposition of Pake-doublets corresponding to deuterons on each segment along the length of the deuterated acyl chain, as shown in Figure 2.8 A. The lower intensity wings (up arrows) correspond to lipids in vesicle regions where the bilayer normal is oriented parallel to the magnetic field and prominent edges (side arrows) correspond to lipids in vesicle regions where the bilayer normal is oriented perpendicular to the magnetic field.

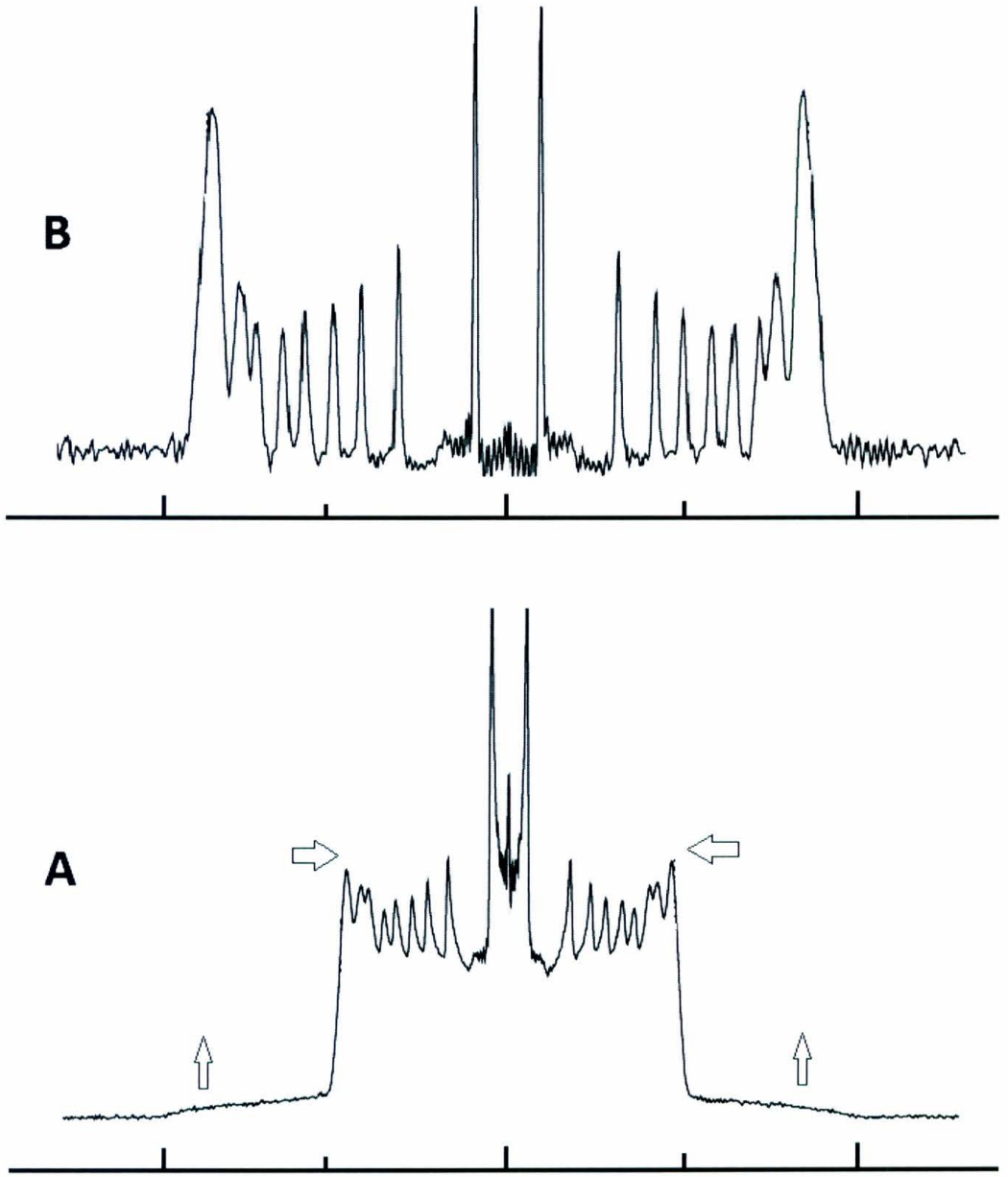

Figure 2.8: A) Deuterium-NMR spectrum of a single-chain-perdeuterated multilamellar vesicle (MLV) sample of POPC-d_{31}/POPG, and B) the corresponding oriented bilayer spectrum obtained by de-Paking of spectrum (A).

2.4 Order parameter profile

The order parameter S_{CD} is directly related to the quadrupolar splitting. S_{CD} reflects the average orientations and motions of the C-D bond vector with respect to the bilayer normal. It is a function of the carbon-deuterium bond angle, θ_n (the angle between the n^{th} carbon-deuterium bond and the bilayer normal) for different segments. For the oriented spectrum shown in Figure 2.6, the order parameter profile can be calculated from the quadrupolar splitting of each doublet using Equation 9 (Sternin et al. 1988, Lafleur et al. 1989).The order parameter profile provides information about area per lipid, length of hydrocarbon chain and the hydrophobic thickness of lipid bilayers (Bloom et al. 1991).

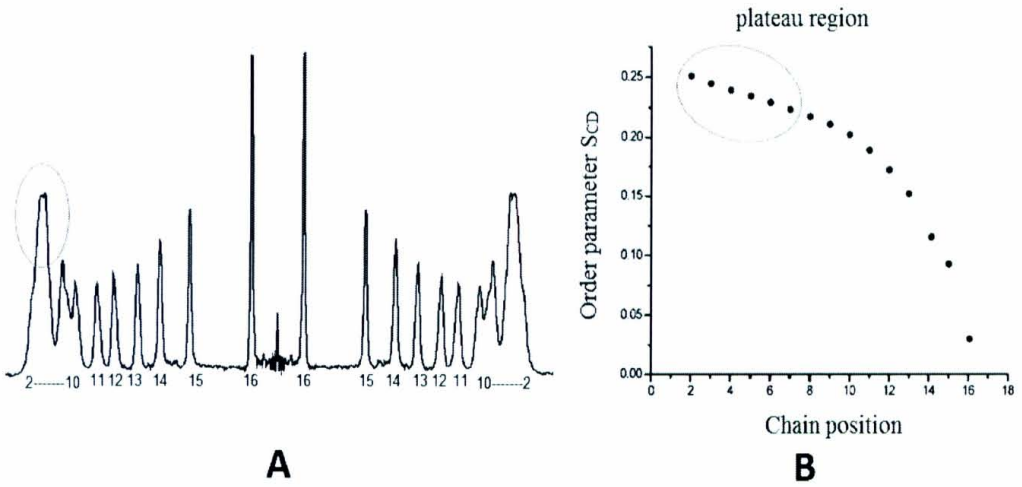

Figure 2.9: Order parameter profile of (A) oriented lipid bilayers composed of POPC-d_{31}/POPG, and (B) the corresponding oriented deuterium spectra.

2.5 DePaking

Bloom and co-workers developed a technique in which the unoriented multilamellar vesicle sample spectrum could be transformed to extract the spectrum that

would be expected for a planar oriented bilayer sample. This technique is referred to as DePakeing (Bloom et al. 1981, Sternin et al. 1983). The DePaked ^{2}H spectrum is a superposition of resolved doublets similar to the corresponding oriented sample deuterium spectrum as shown in Figure 2.8 B

2.6 Phosphorous-NMR

^{31}P-NMR is an attractive probe to study the head group conformation and dynamics of phospholipid bilayers (Seelig 1978; Yeagle 1996). The advantage of ^{31}P is that no isotope labeling is necessary. Since the ^{31}P nucleus is of 100% natural abundance, no isotope labels need to be added. ^{31}P-NMR is thus a non-perturbing technique. The phosphorus nucler spin is ½ and its relative sensitivity is 0.06 compared to that of a hydrogen nucleus. The dipole-dipole interactions are very small between ^{31}P and ^{1}H nuclei and are easily removed by application of an appropriate decoupling technique.

The chemical shift of a phosphorous nucleus results from partial shielding of the magnetic field by surrounding electron density and varies as a function of phospholipid head group orientation with respect to magnetic field. In phospholipid molecules, the ^{31}P nucleus is surrounded by four oxygen atoms which are strongly electronegative. This is analogous to a phosphodiester. The electron density around the ^{31}P nucleus is not isotropic due to these electronegative neighbors. The dependence of chemical shift on head group orientation is called Chemical Shift Anisotropy (CSA). The chemical shielding is minimum along the direction of low electron density and maximum along the direction of high electron density. The following description is based on treatments by Seelig (1978) and Smith and Ekiel (1984).

2.6.1 ^{31}P-NMR powder spectra

For a polycrystalline sample, σ_{11}, σ_{22}, and σ_{33} are components of the chemical shift tensor (σ) along the three principle coordinates in an external magnetic field as illustrated in Figure 2.10 A. Polycrystalline samples contain large numbers of randomly

oriented microdomains. The ^{31}P spectrum of a polycrystalline sample is a superposition of lines with chemical shifts corresponding to all possible orientations of a single crystal with respect to the magnetic field. The spectrum for such a sample, in the absence of motion, is illustrated in Figure 2.10 B.

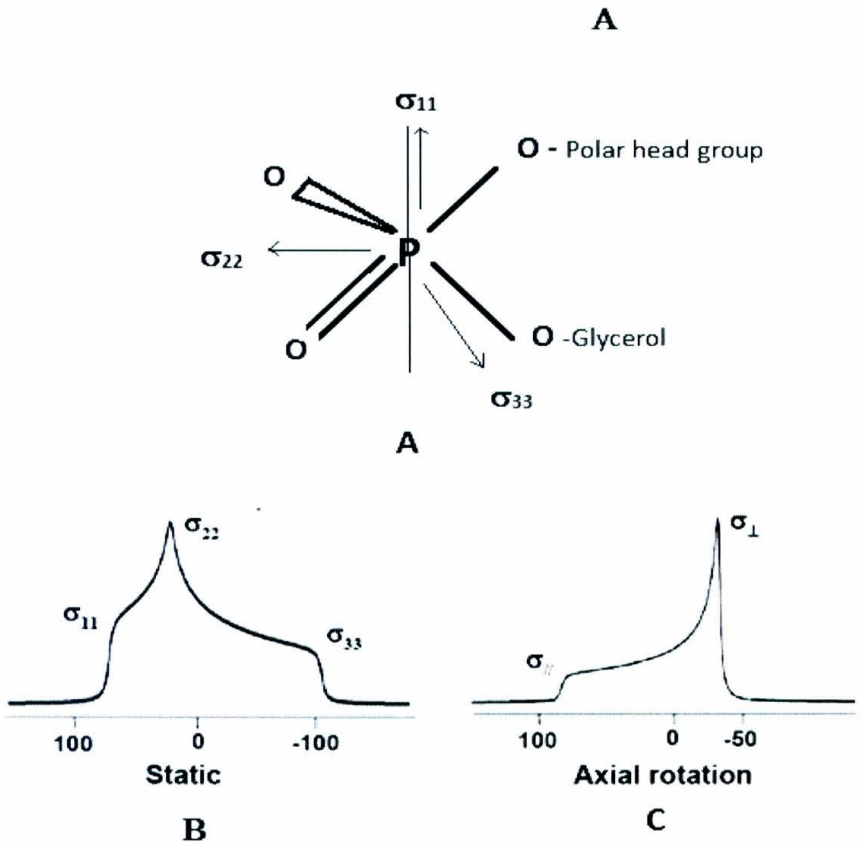

Figure: 2.10: ^{31}P anisotropic chemical shift (powder pattern) spectra of a phospholipid head group. (A) Chemical shift tensor components of a ^{31}P nucleus in the principle coordinate system, (B) ^{31}P-NMR spectrum of a static polycrystalline phosphodiester sample, and (C) ^{31}P-NMR spectrum of a polycrystalline phosphodiester sample containing lipids undergoing rapid axial rotation. Reprinted with permission from *"Anne E Mecdermott, Tatyana Polenova (2010). Solid state NMR Studies of Biopolymers. John Wiley and Sons". Copyright© 2010, John Wiley and Sons.*

In the liquid crystalline bilayer state, lipid molecules undergo fast and axially symmetric reorientations about the bilayer normal. In this state each lipid molecule acts like a tiny single crystal with rotational symmetry about the director axis parallel to the direction σ_{11}. In this context, the director axis is an axis about which lipid molecules undergo motions with rotational symmetry. If there is rapid axial motion about σ_{11}, the resonances are identical when the magnetic field is parallel to the σ_{22} and σ_{33} directions and these components are partially averaged to a single component $\sigma_{\perp}$ which is given by

$$\sigma_{\perp} = \tfrac{1}{2}(\sigma_{22} + \sigma_{33}). \qquad \text{..... (13)}$$

The resulting spectral shape is shown in Figure 2.10 C.

In a sample containing phospholipids undergoing rapid axially symmetric reorientation the chemical shift along the direction of σ_{11} is defined as $\sigma_{//}$ and given by

$$\sigma_{//} = \sigma_{11}. \qquad \text{..... (14)}$$

The chemical shift anisotropy $\Delta\sigma$ is defined as the difference between parallel and perpendicular components of chemical shift tensor and is given by

$$\Delta\sigma = \sigma_{//} - \sigma_{\perp}. \qquad \text{..... (15)}$$

2.6.2 ^{31}P-NMR spectra of oriented lipid bilayers

In the liquid crystalline phase for oriented lipid bilayers, all lipids are oriented in a particular direction and thus contribute to a single resonance frequency depending on the direction of the magnetic field. Figure 2.11 illustrates the chemical shifts of samples oriented parallel and perpendicular to the magnetic field. For parallel orientation, the resonance corresponds to the $\sigma_{//}$ component as shown in Figure 2.11 A and for the perpendicular orientation the resonance corresponds to the $\sigma_{\perp}$ component as shown in Figure 2.11 B.

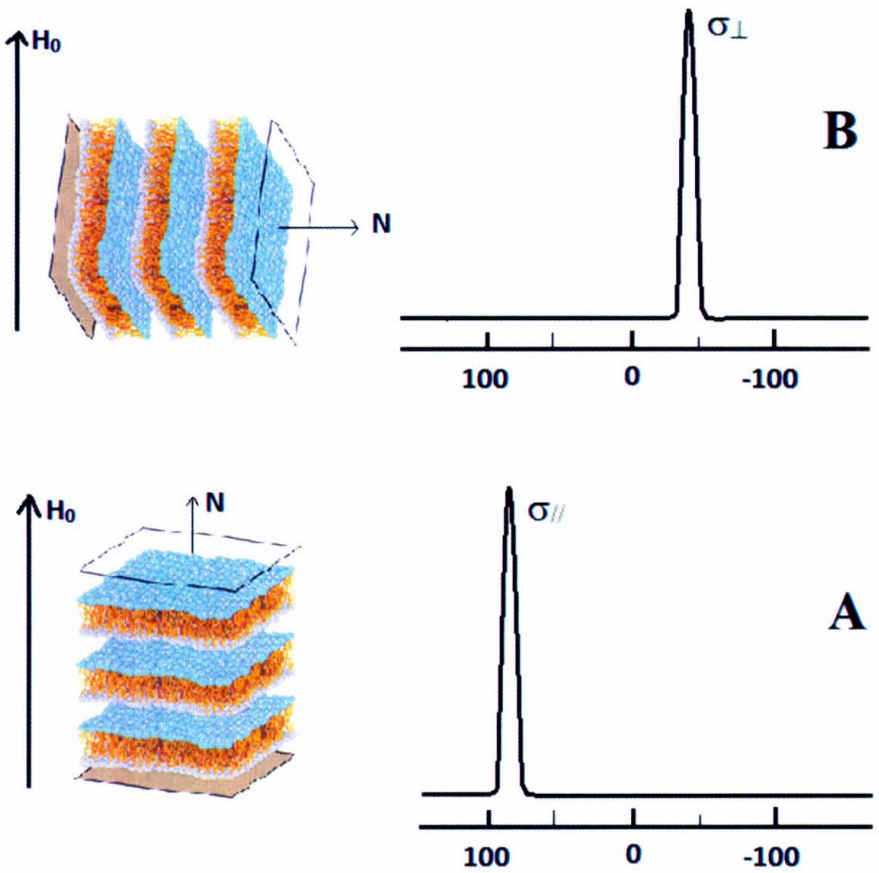

Figure 2.11: A) ^{31}P-NMR spectrum of an oriented bilayer with its normal oriented parallel to magnetic field, and B) ^{31}P-NMR spectrum of an oriented bilayer with its normal oriented perpendicular to magnetic field.

Chapter 3

Materials and Methods

3.1 Materials

3.1.1 Lipids and peptides

Phospholipids used to prepare oriented and vesicle samples included single-acyl-chain-perdeuterated POPC-d_{31} (1-palmitoyl-d_{31}-2-oleoyl-*sn*-glycero-3-phosphocholine), POPG (1- palmitoyl-2-oleoyl-*sn*-glycero-3 phospho-(1'-*rac*-glycerol) and double-acyl-chain-perdeuterated DPPC-d_{62} (1, 2 dipalmitoyl-d_{62}-*sn*-glycero-3-phosphocholine). All phospholipids were obtained from Avanti Polar Lipids (Alabaster, AL) and used without further purification. Egg PG and $CaCl_2$ were purchased from Sigma Aldrich Laboratory (Oakville, ON). BLES (Bovine Lipid Extract Surfactant), a clinically used surfactant in saline dispersion was received as a donation from BLES Biochemicals (London, ON). $CHCl_3$ (Chloroform) and MeOH (Methanol) were purchased from the Fisher Scientific Company. Deuterium-depleted water was purchased from Cambridge Isotopes Laboratory (Andover, MA). Muscovite mica (grade V-4, Dimension 75×25×0.26 mm^3) was purchased from Structure Probe (West Chester, PA). This mica was cut into smaller pieces with dimensions of 0.5×1.2cm^2 (unless otherwise mentioned) and a thickness of about 50μm.

Mini-B is a disulfide-linked construct of both N-term (8-25) and C-term (63-78) regions of SP-B with an amino acid sequence of CWLCRALIKRIQAMIPKG-GRMLPQLVCRLVLRCS (Waring et al 2005). The peptide was prepared chemically via solid-phase methods employing O-fluorenylmethyl-oxycarbonyl (Fmoc) chemistry by Alan Waring (UCLA) (Booth et al. 2004). Organic solvents and other reagents used for Mini-B peptide synthesis and purification were high-performance liquid chromatography (HPLC) grade or better. The peptide was assembled on a prederivatized N-Fmoc-O-tert–butylserine HMP resin (AnaSpec). Deprotection and cleavage of the peptide from the resin were carried out, followed by cold precipitation with tert-butyl ether. The crude product was then purified by preparative reverse phase HPLC with a Vydac C-18 column. The molecular weight of the peptide was confirmed by fast atom bombardment or MALDI-TOF mass spectrometry and its > 95% purity determined by analytical HPLC.

The disulfide linkages were formed by air-mediated oxidation of the peptide in structure-promoting solvents (Waring et al. 2005). The peptide was lyophilized and stored in a refrigerator at 4 °C. The N-terminal segment (CWLCRALIKRIQAMIPKG) of Mini-B was prepared in the same way. The C-terminal segment (GRALPQLVCRLVLRCSM) of Mini-B was expressed as a recombinant protein in E.coli purified and using the approach described by Lindhout and co-workers (Lindhout et al. 2003).

3.1.2 Mica plates

Muscovite mica ($KAl_2(Si_3Al)O_{10}(OH,F)_2$) was used to prepare mechanically oriented lipid bilayer samples. It was cut into required dimensions and cleaved to be as thin as possible. Since thin mica plates are very fragile, they were handled very gently while preparing the oriented bilayer sample. Freshly cleaved mica plates were used within an hour or two to avoid dust accumulation on plates. Mica surfaces possess anionic charge. Due to its charged nature, mica can easily orient the phospholipids in such a way that the hydrophilic head group interacts with the anionic mica surface (Rainey and Syles 2005).

3.2 Methods

3.2.1 Preparation of mechanically oriented lipid bilayer samples

Mechanically oriented lipid bilayers were prepared on mica plates by depositing solutions of lipid or lipid with peptide in organic solvent (Yang et al. 2009). The procedure was as follows: muscovite mica plates were cut into 0.5cm×1.2cm rectangles for each sample. Then, 9 mg of POPC-d_{31}/POPG (7:3) dry powder was weighed out using a Mettler balance. The lipids were dissolved in 150μL of $CHCl_3$/MeOH (1:1). Lipid solution volumes of about 1μL were deposited as a single drop on each freshly cleaved mica plate. Care was taken not to spread the lipid solution to the boundaries which would result in unorinentation of lipids (powder distribution) by applying solution only in the middle region of the plate. After a cycle of deposition of lipid solution on all 12

plates, the lipid solution was allowed to dry on the mica plates for 3-5 minutes. Lipid solution was again applied in the same fashion to all plates for about ten rounds until all the solution was depleted. Mica plates with deposited lipid were placed in a fume hood overnight to remove the organic solvent; residual organic solvent was removed by keeping the plates in a vacuum desiccator for 6-8 hours to avoid any interference of organic solvent with the lipids. Then, 6μL of deuterium-depleted water (Cambridge Isotopes) was added to each plate after which plates were placed in a sealed chamber containing saturated ammonium phosphate solution (65grams/250mL). The lipids were hydrated at room temperature for four days. Then, all the plates were stacked together and the top plate was covered with an empty plate having the same dimensions. The stacked plates were wrapped with thin plastic film and sealed into an envelope of thick plastic film using a heat sealer. Before sealing, 8-10μL of deuterium-depleted water was added between the thin and thick plastic to prevent the sample drying out while being exposed to high temperature and also to help in maintaining a good hydration level. In order to allow the sufficient time to hydrate the lipids between mica plates the sample was prepared two days before it was placed in an NMR probe.

The BLES, which was received from BLES Biochemicals, was not dry powder. Instead, it was a saline dispersion with a concentration of 22.6 mg/mL as determined by phosphorous assay (Bartlett method). To extract BLES from saline dispersion, the method of Bligh and Dyer (Bligh and Dyer 1959) was used. Then, 9mg (400μL) of saline dispersion BLES was dissolved in 2ml of $CHCl_3$/MeOH (2:1). The mixture underwent phase separation into two liquid phases. The lower, BLES-containing phase was extracted. To enable deuterium-NMR studies, perdeuterated DPPC-d_{62} corresponding to 2.5% of the dry lipid weight was mixed with the organic extract. Also, 1 mol % peptide was added to the lipid for peptide-with-lipid studies. The mixture was then dried under a stream of nitrogen gas for 40-60 minutes. Then, the dried mixture was dissolved with 150μL of CHCl3/MeOH (1:1) and oriented samples were prepared using the method described above.

3.2.2 Preparation of vesicle samples

To prepare multilamellar vesicles, 20mg of dry powder mixtures containing POPC-d_{31}/POPG or POPC-d_{31}/POPG with 1 mol % peptide were dissolved in a round bottom flask. The organic solvent was removed by rotary evaporation. The residual organic solvent was further removed by vacuum drying overnight. To hydrate the mixture, 300-400 µL of deuterium-depleted water was added in steps while rotating the flask to make a homogeneous mixture. The sample was transferred to an NMR tube and sealed tightly with Teflon tape. All the samples were stored in a freezer after use. To prepare multilamellar vesicles with BLES, the above described method was followed after having extracted BLES from saline dispersion.

3.2.3 Preparation of Tubular Myelin samples

A mixture of DPPC: egg PG (7:3) with 13% by weight of SP-B was used for the preparation of tubular myelin. To prepare tubular myelin *in vitro*, we followed the method described in Morrow et al. 2005. The procedure was as follows: 1.75 mg of DPPC, 0.75 mg of egg PG and 0.373 mg of SP-B were dissolved in $CHCl_3$: MeOH (1:1). The lipid-protein solution was dried under nitrogen gas and placed in a vacuum chamber overnight. The dried mixture was suspended in 2.5 ml of buffer containing 10 mM Tris (pH 7.4), 145 mM NaCl and 1 mM ethylenediaminetetraacetic acid (EDTA) and then hydrated at 40°C for one hour, with frequent vortexing. Then the solution was transferred to a centrifuge tube and centrifuged at 48,000 × g for 30 minutes. The supernatant was removed and 300 µl of supernatant was added back to the pallet. The phosphorous concentration was determined using Bartlett method. For a sample containing 350 µg of total phospholipid and SP-B, 0.1 mg of SP-A was added with a dry weight of 28%. Then sample was incubated at 37 °C for one hour. Calcium chloride ($CaCl_2$) was added to give a final concentration of 5 mM. Then sufficient double distilled water was added to the sample to give a final volume of 500 µl. The sample was then incubated at 37°C overnight. The sample was then fixed for Transmission Electron Microscopy (JEOL 1200EX Philips 300) at the Electron Microscopy/Flow Cytometry Unit, Faculty of Medicine, Memorial University.

Another sample was prepared in the same way as described above, but with SP-B replaced by 0.093 mg of Mini-B to give the same molar ratio.

3.2.4 Solid-State NMR Analysis

^{2}H-NMR spectra for oriented and multilamellar vesicle samples were acquired at 400 MHz using a locally-assembled 9.4T spectrometer. Data were obtained for oriented and vesicle samples using a horizontally mounted flat coil and a cylindrical coil respectively. For oriented bilayers, the sample was inserted into the probe such that the bilayer normal (N) was parallel to the direction of external magnetic field (B). The temperature for all POPC-d_{31}/POPG and BLES sample spectra was regulated at 23°C and 35°C, respectively.

For deuterium-NMR studies, to avoid a problem with preamplifier recovery time a quadrupolar echo sequence ($\pi/2_y$—τ—$\pi/2_x$—τ) was applied (Davis et al. 1976). Application of a second $\pi/2$ pulse after time τ delays the formation of the echo maximum until time 2τ, allowing sufficient time for the preamplifier to recover and start data collection. These two $\pi/2$ pulses were separated by a 30μs time delay with a pulse length of 4 - 4.25μs. A repetition time of 0.9 s was used.

Deuterium-NMR spectra of POPC-d_{31}/POPG and BLES samples with and without peptide were obtained by averaging of 10,000-50,000 and 200,000-300,000 transients, respectively, without application of any line broadening. Free induction decays were collected with a fixed digitizer dwell time of 1μs because that is the only option for that digitizer. They were then contracted to give an effective dwell time of 4 microseconds because that corresponds to a spectral width of 250 kHz, which is appropriate for a liquid crystalline spectrum. The time domain signal (FID) was then Fourier transformed to obtain the frequency domain spectrum.

For phosphorous (^{31}P) NMR studies of oriented and unoriented samples, all experiments were performed on a Bruker Avance II 14.1 T (600MHz) spectrometer operating at 243.01 MHz for ^{31}P nuclei. Phosphorous chemical shift frequencies were referenced externally relative to 85% H_3PO_4, which appears as an isotropic peak at 0 ppm. For all ^{31}P studies, the sample was inserted in a dual-tuned cross polarization flat-coil probe. For oriented lipid bilayer studies, the sample was inserted in the flat coil probe such that the bilayer normal was oriented parallel to the external magnetic field. ^{31}P chemical shift spectra were obtained by applying high power 43 kHz proton-decoupling. For these experiments, spectral width was 395 ppm, the $\pi/2$ pulse length was 11.5 μs, and the recycle delay was 5 s. Depending on the signal-to-noise ratio, 4000-10,000 transients were averaged for each ^{31}P spectrum.

3.2.5 Order parameter profile

For oriented spectra, such as in Figure 2.9, the order parameter values were calculated using the smoothed order parameter profile approach (Lafleur et al. 1989). The quadrupolar splitting is assigned to each position along the from carbon positions C16-C2. The C1 position does not contain any hydrogens. The carbon positions from C16-C11 are well resolved and thus order parameter values are directly calculated from the quadrupolar splitting using the Equation 9. The quadrupolar splittings for positions C10-C2 overlap each other, however, and thus cannot be directly calculated. To estimate the quadrupolar splitting in the overlapped region the total area under the curve from C10-C2 is equally divided into 9 parts and the frequency from mid-points of each interval are calculated. Then order parameter values are estimated from quadrupolar splittings. The order parameter profile was then drawn as a function of carbon position along the chain as shown in Figure 2.9.

Chapter 4

Results

4.1 Oriented lipid bilayers

In order to study the effect of the SP-B peptide fragments Mini-B, and the combination of SP-B_{CTERM} and SP-B_{NTERM} on model lung surfactant lipid bilayers, we used two types of model lipid bilayer systems: mechanically oriented lipid bilayers and multilamellar vesicle (MLV) lipid bilayers. Oriented and MLV samples were prepared using both POPC-d_{31}/POPG (7:3) and BLES. Mechanically oriented lipid bilayers have lipids aligned in a particular direction whereas multilamellar vesicles are approximately spherical assemblies of concentric lipid bilayers, which can be represented as onion-like structures. Solid-state deuterium (^{2}H) NMR and phosphorous (^{31}P) NMR were used to study the orientation and dynamics of these lipid bilayers in presence and absence of the SP-B peptides. Solid-state ^{2}H-NMR and ^{31}P-NMR spectra can suggest membrane perturbation caused by the peptide via the following kinds of observations:

1. changes in deuterium quadrupolar splitting suggesting changes in orientational order of lipid bilayers;
2. superposition of a Pake-doublet component with smaller splitting suggesting the formation of an unoriented fraction;
3. changes in the line width which can indicate a change in mosaic spread of the oriented lipid bilayer; and
4. changes in ^{31}P chemical shift which can suggest a change in phospholipid head group orientation.

The composition of the POPC/POPG (7:3) oriented lipid bilayers was chosen to mimic the anionic and unsaturated lipid content in lung surfactant and to enable comparison with other studies. The PC/PG (7:3) ratio has been used extensively for previous lung surfactant studies (Russell-Schulz et al. 2009, Farver et al. 2010). Though DPPC is of particular importance for lung surfactant function, its liquid crystalline phase is only found above 44 °C (~40 °C in DPPC-d_{62}). An oriented sample based on DPPC-d_{62} would thus need to be studied above 40 °C, which could result in dehydration of the

sample. For this reason, we chose to use POPC-d_{31} rather than DPPC-d_{62} as the deuterated PC component for our oriented sample studies. The first step in this work was to identify optimal conditions for the preparation of well-oriented lipid bilayer systems.

4.1.1 Hydration of POPC-d_{31}/POPG oriented lipid bilayer sample

Figure 4.1 shows the ^{2}H-NMR spectra collected during the progressive hydration of mechanically oriented lipid bilayers composed of POPC-d_{31}/POPG (7:3) from the time the lipid bilayers were first sandwiched between the mica plates. All ^{2}H-NMR spectra in Figure 4.1 are characteristic of fast and axially symmetric motions of the phospholipids about the bilayer normal. The first deuterium-NMR spectrum was collected two hours after initial preparation of the sample. This spectrum is broad and poorly resolved. This implies that the lipids in the sample were not fully hydrated even though they were oriented between the plates as indicated by the large splittings observed. Successive ^{2}H spectra in Figure 4.1 show that the quadrupolar splitting continuously decreased with time and that resolution improved. This likely means that the number of water molecules forming hydrogen bonds around the phospholipid head group increased with time. As hydrogen bonds around phospholipids increase, the lateral distance between two phospholipids increases and quadrupolar splitting decreases. The decreased quadrupolar splitting implies larger amplitudes of chain motion in the plane of the bilayer and larger lateral area per lipid. The spectra at 30 hours and afterwards (not shown) were stable, indicating an unchanging hydration level. It was found that the average time to completely hydrate an oriented POPC-d_{31}/POPG (7:3) sample was about 30 hours, and all subsequent experiments were performed after allowing the sample hydration to equilibrate for two days following preparation of sample.

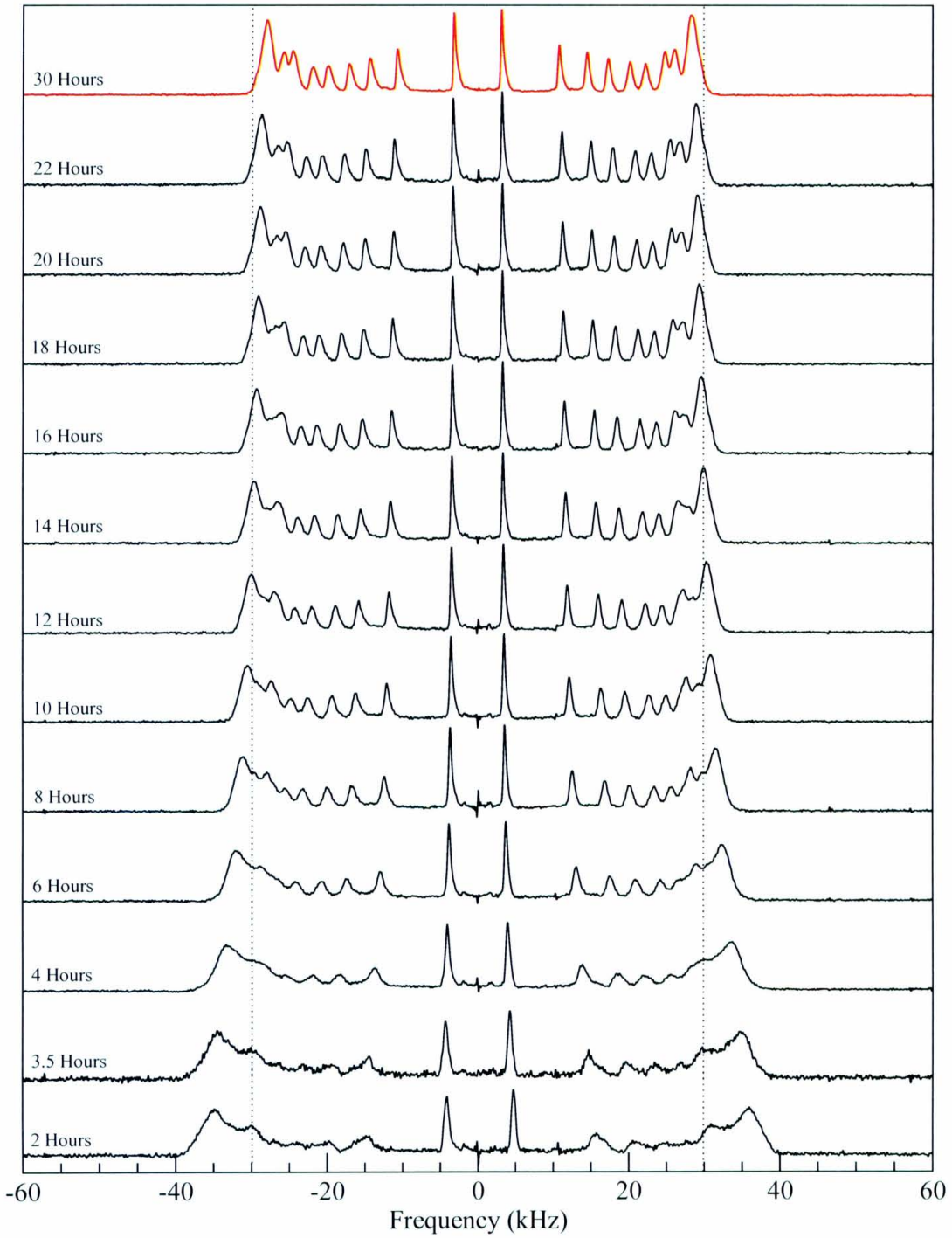

Figure 4.1: ^{2}H-NMR spectra showing the evolution of hydration with time for mechanically oriented lipid bilayers composed of POPC-d_{31}/POPG (7:3).

4.1.2 ^{2}H-NMR of POPC-d_{31}/POPG (7:3) oriented lipid bilayers samples

Deuterium-NMR spectra in Figure 4.2 show that the quadrupolar splitting depends slightly on the amount of lipid sample per plate and on the area of the sample deposited on mica plates for the same hydration conditions. Spectra B, C and D show that the quadrupolar splitting decreased with increasing amounts of sample per plate for a fixed size of plates (0.5cm×1.2cm). The spectrum 'A' shows that the quadrupolar splitting further decreased and that line widths were narrower when larger mica plates (1.2cm×1.2cm) were used. The reduced line widths (sharper peaks) in spectrum 'A' imply less mosaic spread, which is defined as the disorientation between different domains of oriented phospholipid molecules in a sample of mechanically oriented lipid bilayers. In order to verify the expected quadrupolar splitting of a fully hydrated oriented sample, we also prepared a multilamellar vesicle (MLV) sample with the same composition and conditions as the oriented lipid samples. The deuterium spectra for a vesicle (MLV) sample containing POPC-d_{31}/POPG is a superposition of Pake doublets corresponding to each deuteron along the length of the acyl chain. The quadrupolar splittings for all positions along acyl chain were extracted and transformed to give the corresponding oriented sample spectrum in a process known as dePaking (Sternin et al. 1983). Spectrum 'E' is for a vesicle sample dePaked to give the spectrum corresponding to orientation of the bilayer normal parallel to the magnetic field. It is observed that the quadrupolar splittings of vesicle sample 'E' match the quadrupolar splittings of oriented sample 'A'. This means that phospholipid molecules in oriented sample 'A' have the same area per lipid as that of a vesicle sample 'E'.

We can illustrate the same results using smoothed orientational order parameter profiles. Figure 4.3 shows deuterium order parameter profiles of the same oriented samples 'A-E'. Order parameter profile is another way of quantifying the quadrupolar splitting of deuterium probes along the length of the phospholipid acyl chain (Sternin et al 1988). The order parameter S_{CD} of the C-D bond can be directly calculated from quadrupolar splitting $\Delta\nu$ using Equation 9. Comparison of the orientational order

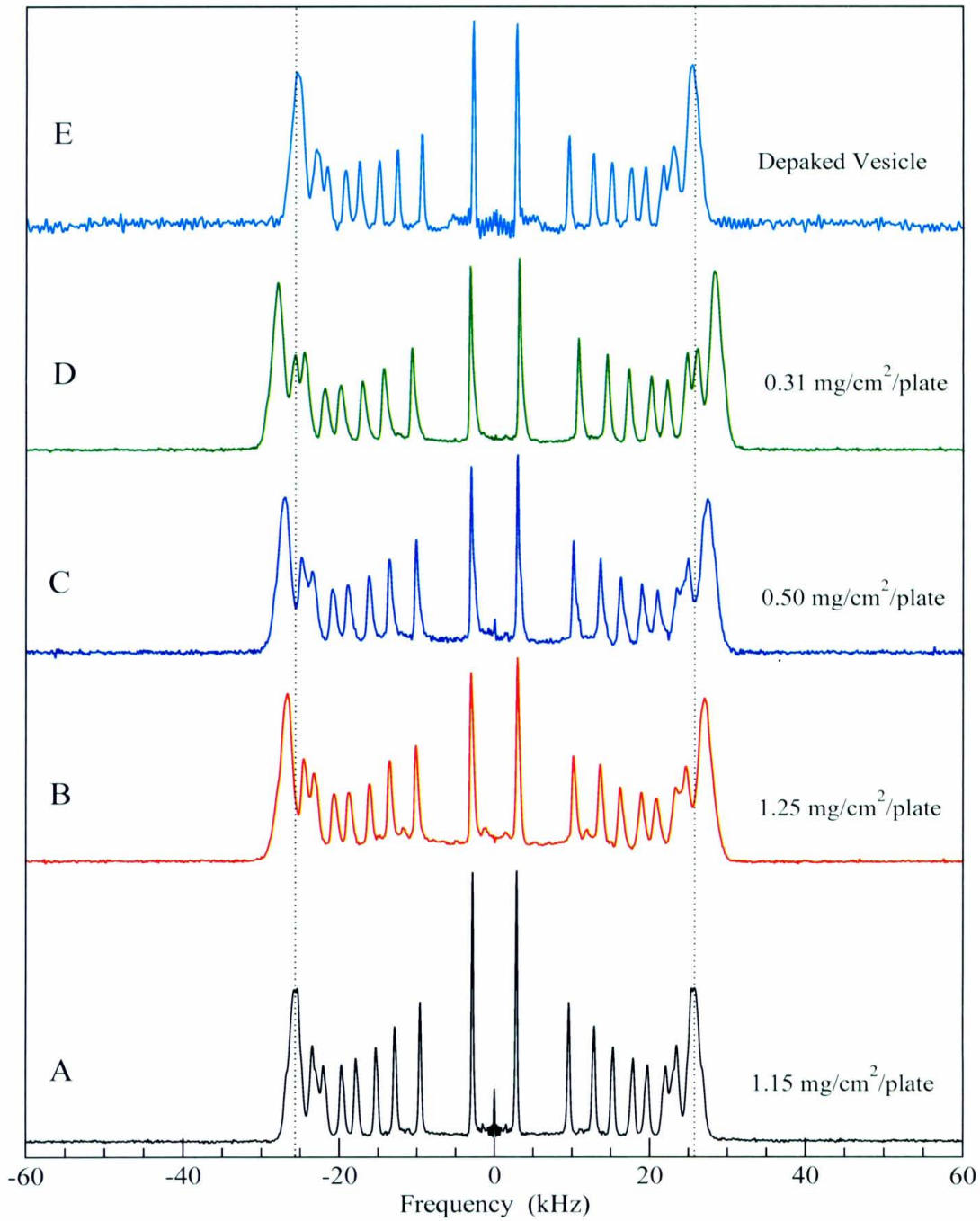

Figure 4.2: ^{2}H-NMR spectra of oriented POPC-d_{31}/POPG bilayers with variable amounts of sample on different sized mica plates (A-D) and of a vesicle sample (E). The quadrupolar splitting of the oriented sample (A) matches that of the dePaked spectrum for vesicle sample (E).

parameter profiles in Figure 4.3 indicates that the ordering of lipids in oriented samples depends on the amount of sample (thickness) between the plates. Samples with higher thickness showed less order than samples with lesser thickness. This may indicate that bilayers near the mica surface have a smaller area per lipid than the bilayers in the middle of the sample possibly due to an enhanced influence from the electric field near the mica plate. Thus the resultant quadrupolar splitting for a thicker sample is reduced in comparison to the thinner sample. As discussed above, the smaller order found with the thicker layers appears to be more representative of full hydration.

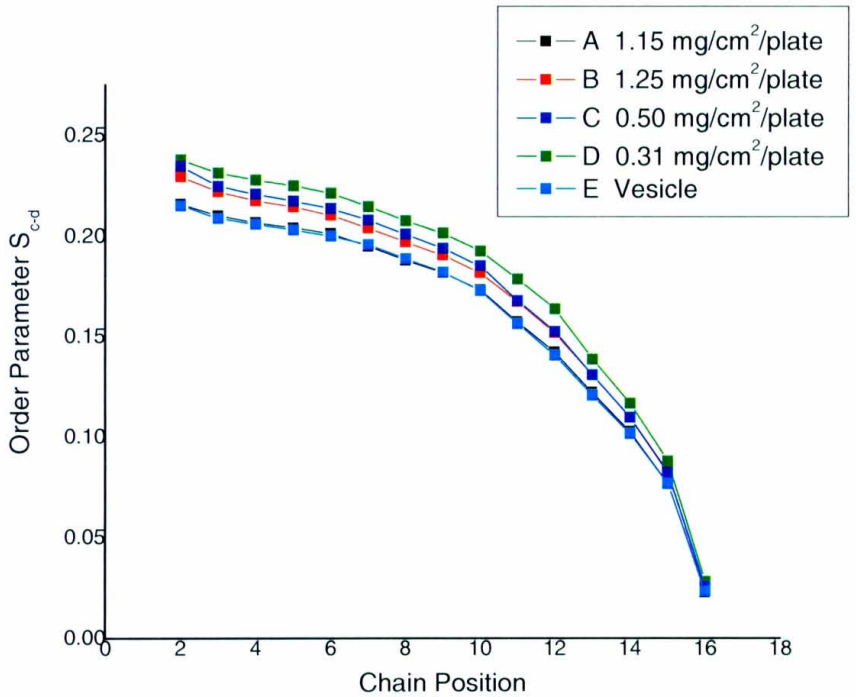

Figure 4.3: ^{2}H-NMR order parameter profiles of oriented POPC-d_{31}/POPG with variable amount of sample per plate extracted from the spectra in 4.2. (Error bars are smaller than the symbol size).

4.1.3 Effect of sample preparation differences on ^{2}H-NMR spectra of oriented lipid bilayer samples containing POPC-d_{31}/POPG and POPC-d_{31} with 1 mol % Mini-B

In order to learn how to prepare well-oriented lipid bilayer samples in the presence of peptide (Mini-B), we tested a number of samples prepared with different numbers of mica plates and plate sizes. In Figure 4.4, spectrum 'A' is for a sample of POPC-d_{31}/POPG with 1 mol % Mini-B on 12 plates with dimensions 0.5cm×1.2cm. The presence of additional intensity between ~+/- 12 kHz in this spectrum shows that Mini-B disrupted the oriented lipid bilayer structure and induced random orientation in part of the sample. The additional intensity between ~+/- 12 kHz is consistent with Pake-doublet intensity at half of the oriented quadrupolar splitting. In order to determine the extent to which the electrostatic interaction between the anionic POPG and cationic Mini-B promoted the perturbation, Sample B was prepared using only POPC-d_{31} with 1 mol % Mini-B. There was, however, no reduction in the additional intensity indentified as corresponding to unoriented bilayers in Sample 'B' compared to Sample 'A', as shown in Figure 4.4. However, the reduced quadrupolar splitting that resulted from the removal of POPG from the mixture suggests an increase of lateral space between lipid molecules, resulting in a larger amplitude of motion of the acyl chains. To see the effect of increasing the number of mica plates while maintaining the same amount of sample, Sample 'C' was prepared with the number of plates increased from 12 to 26, and the plate size set to 0.7cm×1.2cm. Interestingly, this reduced the unorientation caused by peptide. We further increased the number of plates to 40, but no further significant reduction in unorinentation was observed.

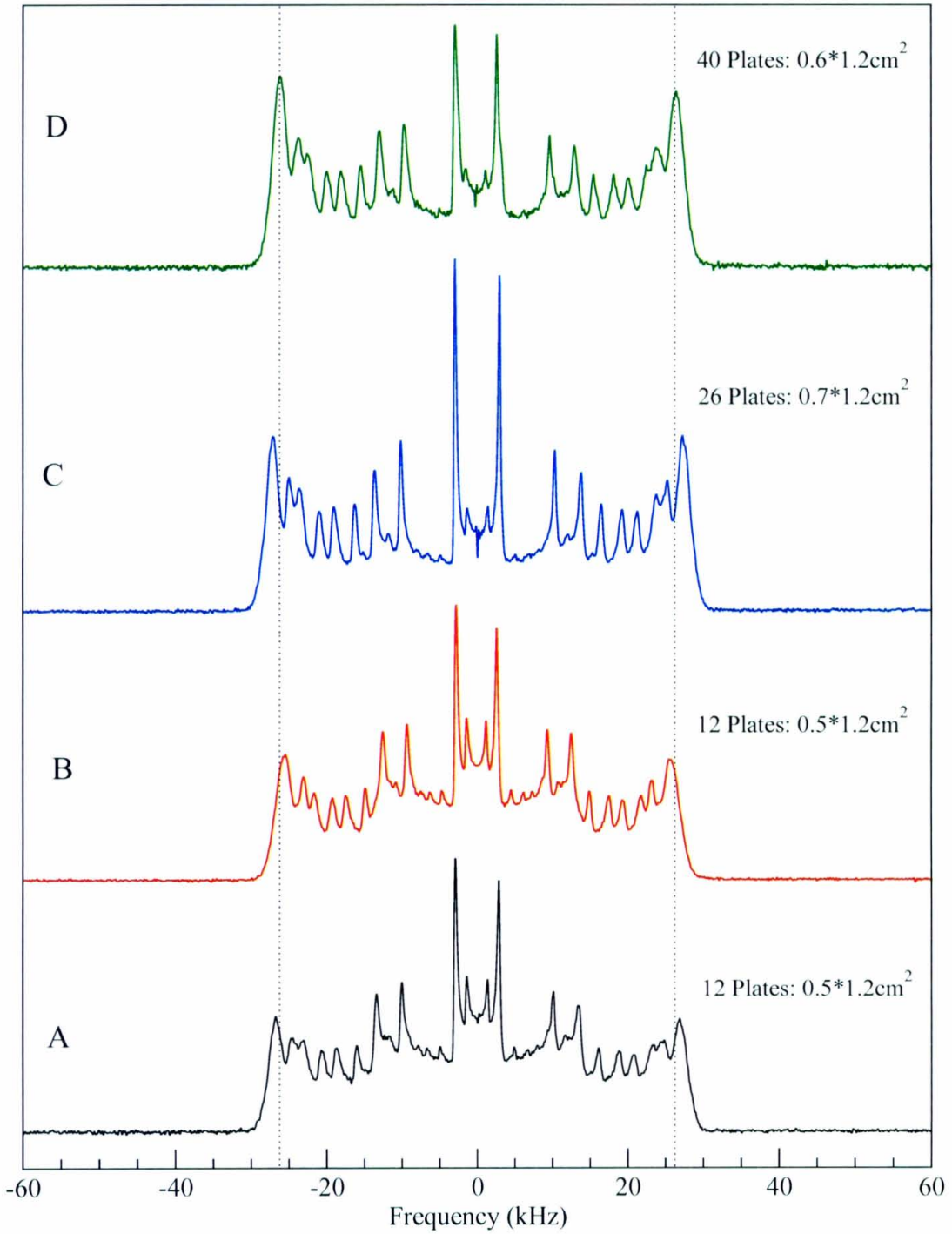

Figure 4.4: ^{2}H-NMR spectra of oriented POPC-d_{31}/POPG (7:3) with 1 mol % Mini-B (A, C and D) and POPC-d_{31} (B) with 1 mol % Mini-B.

4.1.4 Comparison of the effects of Mini-B and Super Mini-B on oriented POPC-d_{31}/POPG (7:3) bilayers

Super Mini-B includes the 7 residue sequence from the N-terminal end of natural SP-B to Mini-B. In order to see if this sequence alters the effect of Mini-B on bilayer orientation, a mechanically oriented bilayer sample containing Super Mini-B (prepared and kindly made available by Mahzad Sharifamadian) was also examined. Figure 4.5 shows that both Mini-B and Super Mini-B perturb the bilayer structure of oriented samples composed of POPC-d_{31}/POPG (7:3). The unoriented fraction caused by both of these peptides is of same order of magnitude as can be seen from the additional intensity at splittings equal to half of the quadrupolar splitting for corresponding features in the oriented bilayer. However, the reduction in quadrupolar splitting of the oriented fraction caused by Super Mini-B is more compared to that caused by Mini-B. This indicates that the effect of Super Mini-B on the oriented fraction of mechanically oriented lipid bilayer is more in comparison to that of Mini-B. Figure 4.6 shows the deuterium order parameter profiles of the same samples as in Figure 4.5. The order parameter profiles tell us that Super Mini-B induces more disordering of lipids than Mini-B in the oriented fraction of oriented lipid bilayers, presumably due to its seven extra amino acid sequence at the N-terminus.

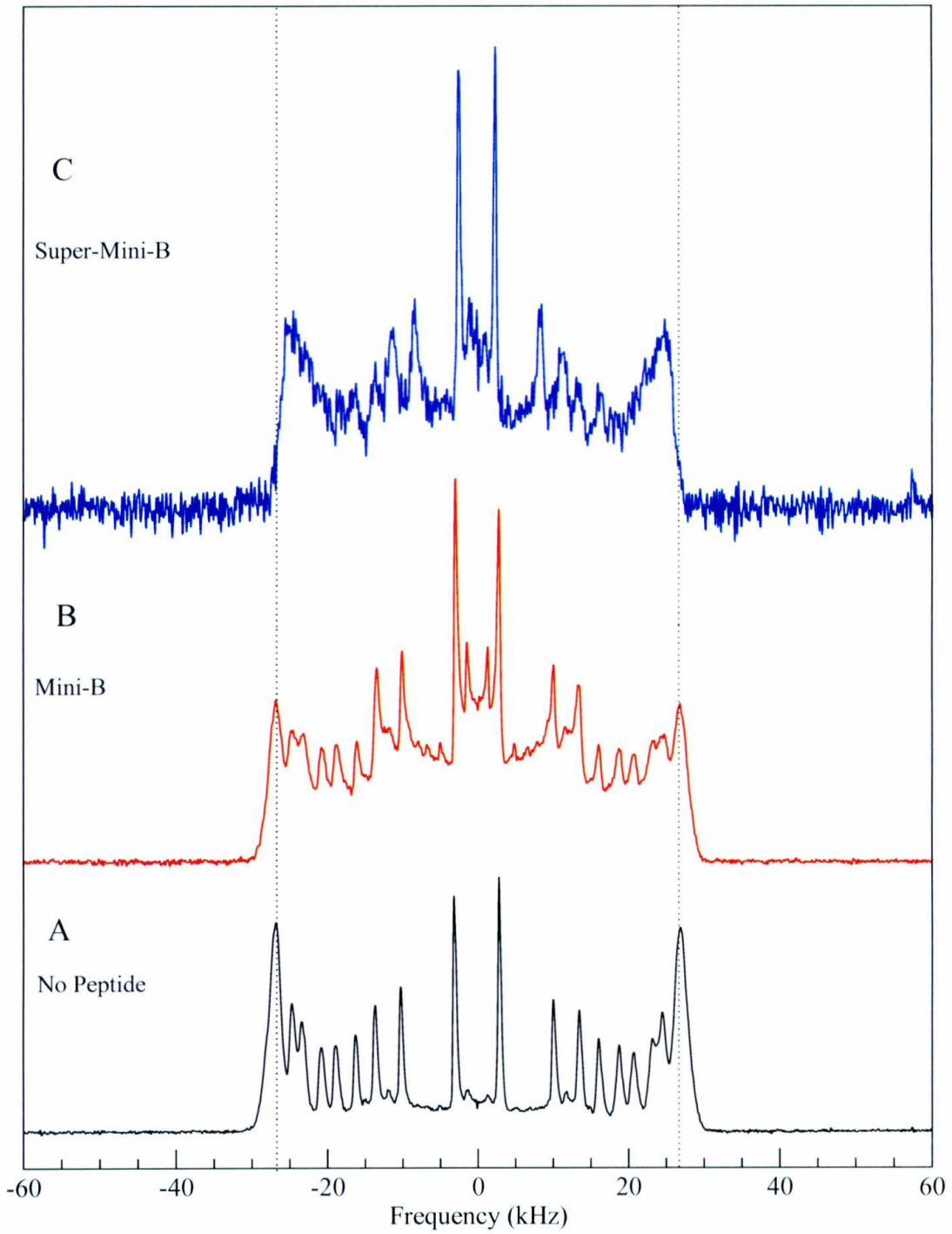

Figure 4.5: ^{2}H-NMR spectra of (A) oriented POPC-d_{31}/POPG (B) oriented POPC-d_{31}/POPG with 1 mol % Mini-B and (C) oriented POPC-d_{31}/POPG with 1 mol % Super Mini-B

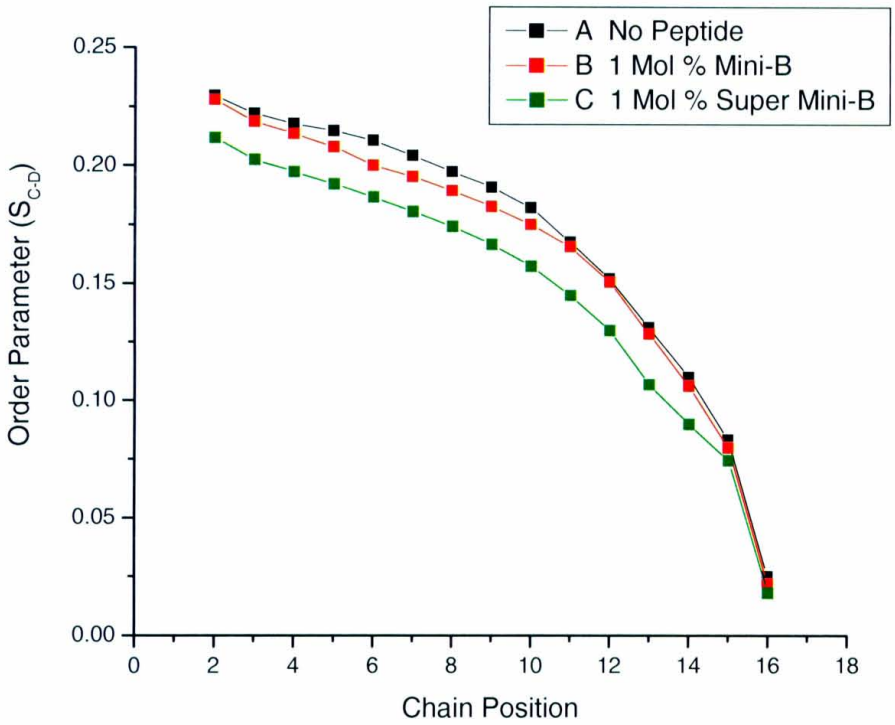

Figure 4.6: ^{2}H-NMR order parameter profiles A) oriented POPC-d_{31}/POPG, (B) oriented POPC-d_{31}/POPG with 1 mol % Mini-B and (C) oriented POPC-d_{31}/POPG with 1 mol % Super Mini-B. (Error bars are smaller than the symbol size).

4.1.5 Comparison of the effects of Mini-B and SP-B_{CTERM} +SP-B_{NTERM} on oriented POPC-d_{31}/POPG (7:3) bilayers

In order to compare the interactions of lung surfactant peptides, Mini-B or the combination of SP-B_{CTERM} and SP-B_{NTERM} with lipid bilayers, oriented lipid bilayers composed of POPC-d_{31}/POPG (7:3) were prepared. We employed solid-state NMR spectroscopy (especially ^{2}H-NMR and ^{31}P-NMR) to study the lipid-protein interactions.

Figure 4.7 shows the ^{2}H-NMR spectra of oriented POPC-d_{31}/POPG (7:3) with and without 1 mol % SP-B peptides. The deuterium spectrum for the sample with no peptide, Figure 4.7A, shows that the lipids in the sample are uni-axially oriented with the bilayer normal parallel to the direction of the magnetic field. No fraction having random bilayer normal directions was found. The sample with 1 mol % Mini-B (Spectrum 'B') shows that Mini-B perturbed the bilayer structure and induced a fraction of sample having randomly oriented bilayer normals into the oriented lipid bilayer sample. As described above the observation of Pake-doublets with quadrupolar splittings at half of the corresponding oriented component quadrupolar splitting is a characteristic of the presence of an unoriented fraction in oriented bilayers. The addition of 1 mol % Mini-B to oriented lipid bilayers did not significantly reduce the quadrupolar splitting, but did change the line width of the quadrupolar peaks. The change in line width indicates a change in mosaic spread of lipid bilayer orientations. Spectrum 'C' is for oriented POPC-d_{31}/POPG containing 1 mol % SP-B_{CTERM} and SP-B_{NTERM} together. The combination of SP-B_{CTERM} and SP-B_{NTERM} is similar to Mini-B but without two cross-linked disulphide bonds and with no connection between the two helical domains of SP-B_{CTERM} and SP-B_{NTERM}; from this point onwards in the thesis, this combination of these peptides will be referred to 'SP-B_{CTERM} + SP-B_{NTERM}'. Comparison between the samples with Mini-B and SP-B_{CTERM} + SP-B_{NTERM} gives information about how the presence of these two cross-linked disulphide bonds and the connection between the C-terminal and N-terminal domains modify the effects of Mini-B on oriented bilayers. Unlike Mini-B, addition of 1 mol % SP-B_{CTERM} + SP-B_{NTERM} induced a small fraction of unoriented bilayer in oriented POPC-d_{31}/POPG lipid bilayers but resulted in no significant change in quadrupolar splitting.

Figure 4.8 illustrates the order parameter profiles of oriented samples composed of POPC-d_{31}/POPG with and without SP-B peptides. ^{2}H order parameter profiles give information about the lipid ordering, chain motions, and area per lipid in lipid bilayers. Figure 4.8 shows that both Mini-B and the combination of SP-B_{CTERM} + SP-B_{NTERM} peptides did not significantly alter the shape of the order parameter profiles in comparison to the profile for the sample with no peptide. These order parameter profiles

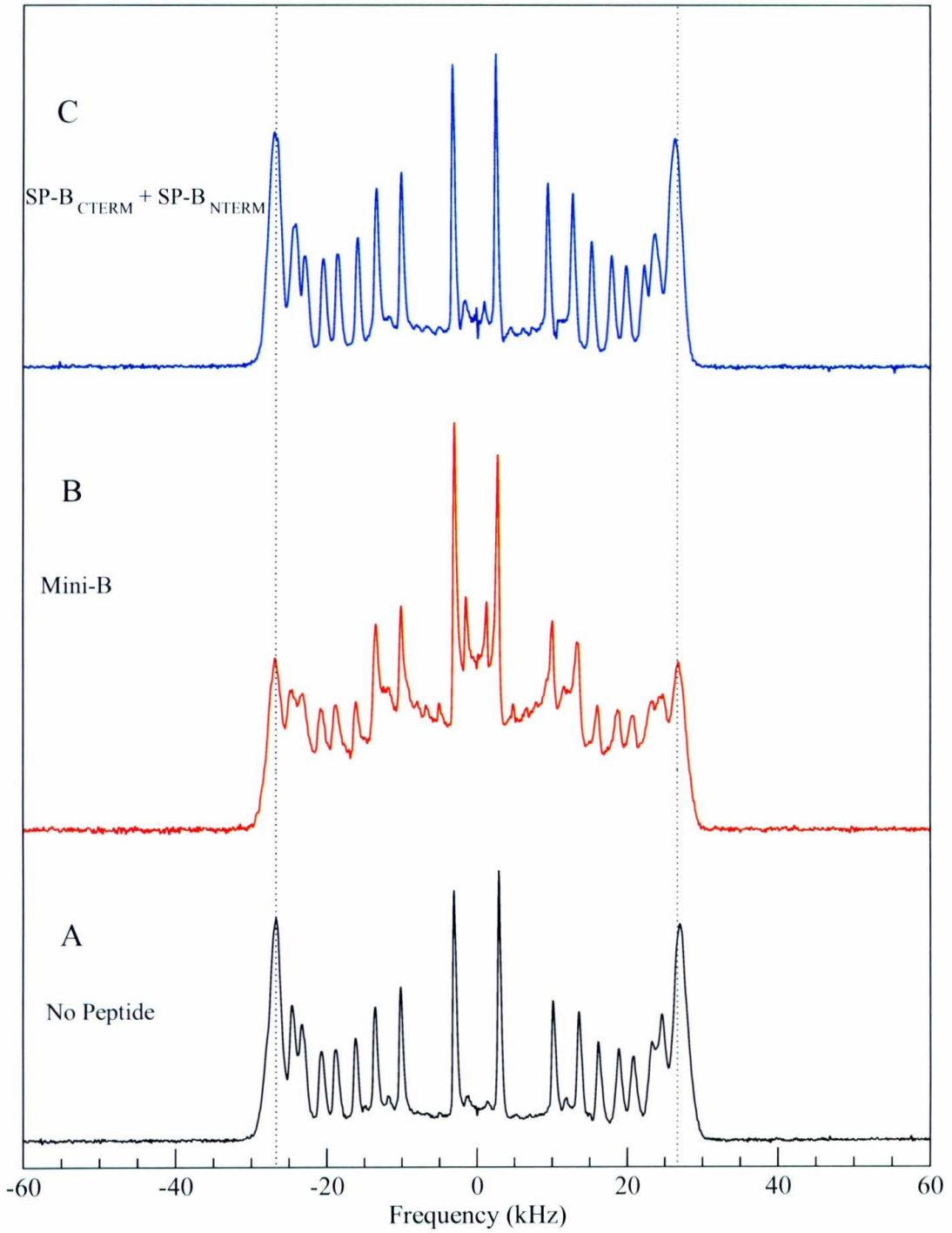

Figure 4.7: ^{2}H-NMR of (A) oriented POPC-d_{31}/POPG, (B) oriented POPC-d_{31}/POPG with 1 mol % Mini-B and (C) oriented POPC-d_{31}/POPG with 1 mol % of POPC-d_{31}/POPG (7:3).

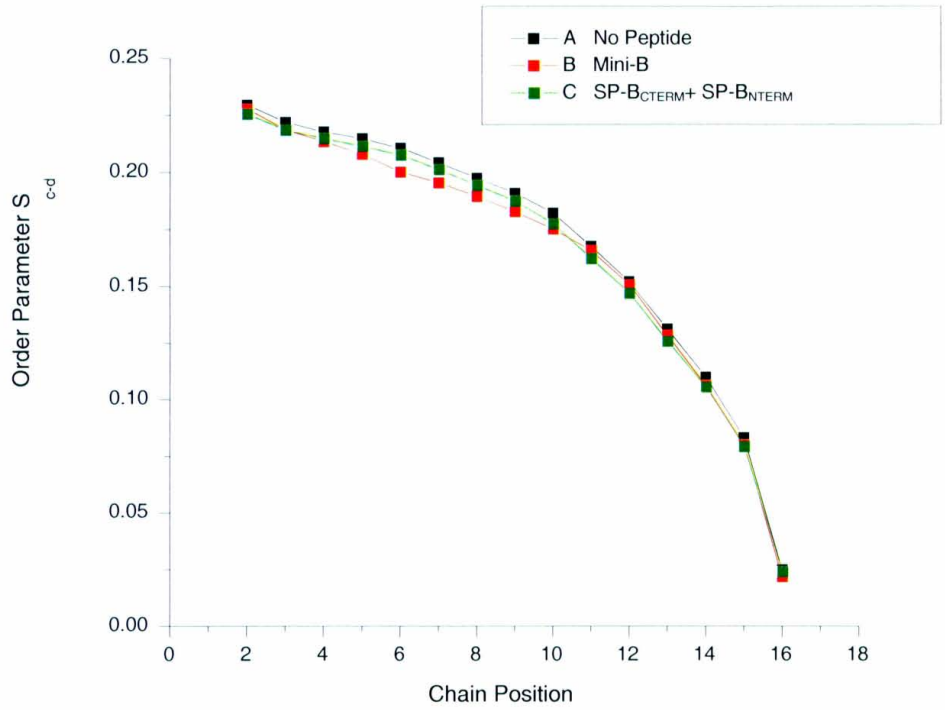

Figure 4.8: ^{2}H-NMR order parameter profiles of A) oriented POPC-d_{31}/POPG (B) oriented POPC-d_{31}/POPG with 1 mol % Mini-B and (C) oriented POPC-d_{31}/POPG with 1 mol % SP-B $_{CTERM}$ + SP-B $_{NTERM}$. (Error bars are smaller than the symbol size).

tell us that Mini-B and SP-B$_{CTERM}$ + SP-B$_{NTERM}$ do not significantly affect the chain orientational order of the oriented fraction of the bilayer. In the presence of SP-B$_{CTERM}$ + SP-B$_{NTERM}$, the oriented lipid bilayers were weakly perturbed. From previous studies of 1 mol % of SP-B$_{CTERM}$ in oriented lipid bilayers (Yang et al. 2009), it was reported that SP-B$_{CTERM}$ alone significantly perturbed the bilayer structure. In the present work, we found that Mini-B perturbed the bilayer similarly to SP-B$_{CTERM}$, but that SP-B$_{CTERM}$ and SP-B$_{NTERM}$ together are not able to perturb the bilayer structure as strongly as SP-B$_{CTERM}$ alone in oriented POPC-d_{31}/POPG bilayers.

The other approach used to study the interactions of these peptides with lipid bilayers was ^{31}P-NMR, which provides information on head group dynamics and structure. Figure 4.9 shows phosphorous spectra for oriented POPC-d_{31}/POPG (7:3) and oriented POPC-d_{31}/POPG (7:3) with 1 mol % SP-B_{CTERM} + SP-B_{NTERM}. The ^{31}P spectrum in Figure 4.9A is for an oriented sample in the absence of peptide. It shows a narrow peak indicating that all lipids have identical orientation with respect to the external magnetic field. The peak at 37.1 ppm is for oriented POPC and the small peak at 32.8 ppm corresponds to oriented POPG with an intensity ratio similar to that of the lipid composition in the sample (Yang et al. 2009). The intensities of these two slightly resolved peaks confirm the relative concentrations of POPC and POPG in the oriented

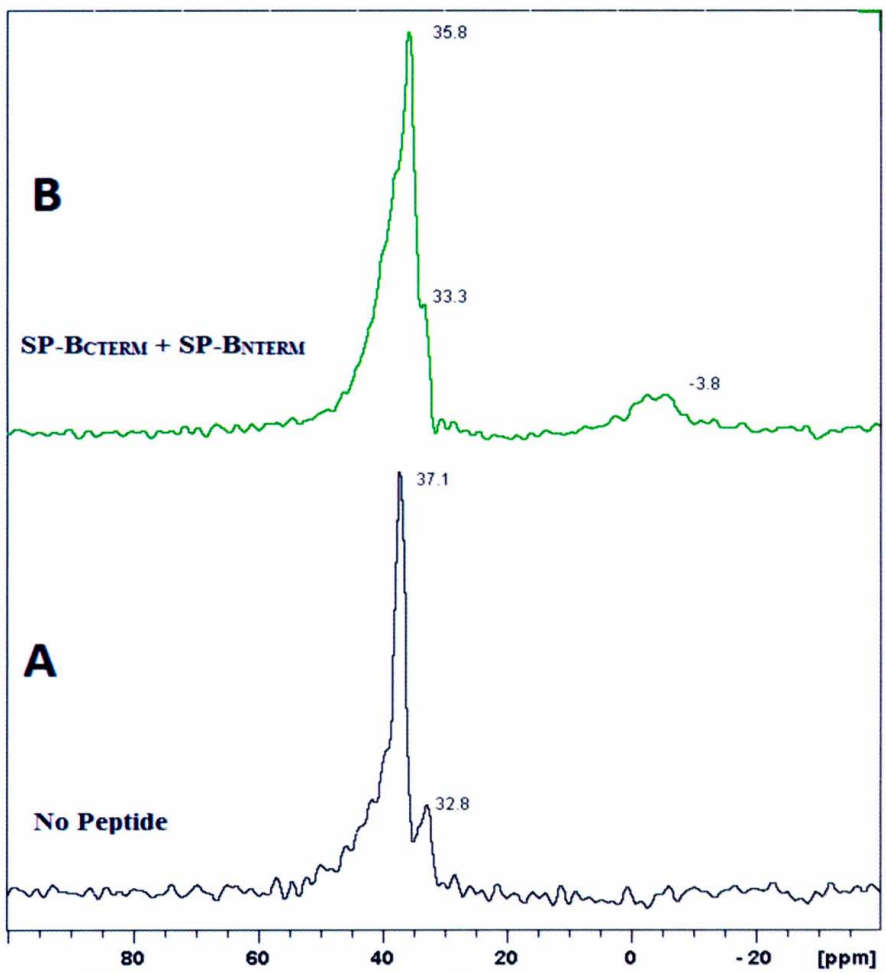

Figure 4.9: ^{31}P-NMR (A) oriented POPC-d_{31}/POPG, and (B) oriented POPC-d_{31}/POPG with 1 mol % SP-B_{CTERM} + SP-B_{NTERM}

sample. The different chemical shifts of phosphorous in PC and in PG are due to the difference in electron density distribution around the phosphorus when the phosphate group is attached to a choline versus a glycerol, as shown in Figure 2.10 A. (No data was taken with Mini-B in oriented POPC-d_{31}/POPG (7:3), due to unavailability of the ^{31}P probe during the time of experiment). The ^{31}P spectrum in Figure 4.9B is for oriented POPC-d_{31}/POPG (7:3) with 1 mol % SP-B_{CTERM} + SP-B_{NTERM}. The spectrum shows that the two peaks corresponding to POPC and POPG are not as well resolved in the presence of 1 mol % SP-B_{CTERM} + SP-B_{NTERM} as in spectrum 'A'. The appearance of a new peak at -3.8 ppm shows that the presence of 1 mol % SP-B_{CTERM} + SP-B_{NTERM} perturbed the lipid bilayer and induced a small fraction of unoriented bilayers. In presence of 1 mol % of peptides, the POPC peak is shifted upfield by 1.3 ppm to 35.8 ppm and the POPG peak shifted downfield by 0.5 ppm to 33.3 ppm. This change in the chemical shift of a peak suggests that peptide interaction with lipids alters the lipid head group conformation in the oriented fraction. Unlike the oriented POPC-d_{31}/POPG in spectrum 'A', the merging of these two peaks may indicate that the POPC and POPG head groups had more similar conformations in the presence of 1 mol % SP-B_{CTERM} + SP-B_{NTERM} in the oriented sample. In theory, if $\sigma_{//}$ is the ^{31}P chemical shift corresponding to the oriented fraction (lipids aligned parallel to the magnetic field) then the chemical shift corresponding to the unoriented fraction (lipids aligned perpendicular to the magnetic field) would be expected to show intensity at $\sigma_{\perp} \approx -\sigma_{//}/2$. The spectrum for the oriented sample with 1 mol % SP-B_{CTERM} + SP-B_{NTERM}, spectrum 'B', shows a peak at -3.8 ppm. This peak position, presumably corresponding to unoriented material, likely indicates that head group orientations in oriented and unoriented fractions of the sample were not the same. If they were, the chemical shift for the unoriented fraction peak would be to be at -17.0 ppm. These results suggest that the combination of 1 mol % SP-B_{CTERM} + SP-B_{NTERM} perturbs the headgroup conformation in POPC-d_{31}/POPG and that the perturbations in the oriented and unoriented fractions are different.

4.1.6 Comparison of the effects of Mini-B and SP-B_{CTERM} +SP-B_{NTERM} on oriented BLES bilayers

Model lipid bilayers composed of POPC-d_{31}/POPG (7:3) gave insights into how SP-B peptides affect the model lipid bilayer structure (Yang et al. 2009). We were also interested in studying lipid-peptide interactions in oriented bilayers composed of a more natural lung surfactant composition. We chose BLES, a clinically-used lung surfactant that contains all components of the lung surfactant system except for the hydrophilic proteins SP-A and SP-D. We prepared oriented samples of BLES doped with 2.5% DPPC-d_{62} incorporated as a probe for solid-state deuterium-NMR studies. Incorporation of 2.5% DPPC-d_{62} is not expected to significantly alter the composition or properties of BLES. Addition of more DPPC-d_{62} might produce a better signal to noise (S/N) of ^{2}H spectrum, but might also perturb the natural lung surfactant composition in BLES. Because lipids in bilayers undergo cooperative collective motions, incorporation of deuterium probes gives information on the local environment of DPPC-d_{62} probes in BLES lipid bilayers.

Figure 4.10 shows ^{2}H-NMR spectra for oriented BLES in the presence and absence of SP-B peptides. The spectrum shown in Figure 4.10A is for oriented lipid bilayers composed of BLES without peptide. The signal-to-noise ratio is poor due to the small fraction (2.5%) of perdeuterated DPPC incorporated in the BLES. The spectrum in Figure 4.10A shows that the sample is well oriented despite the presence of a complex mixture of lipids (saturated and unsaturated lipids). The small amount of extra intensity seen at half the quadrupolar splittings of the oriented fraction doublets is evidence of the existence of a small fraction of unoriented bilayers presumably caused by presence of native hydrophobic surfactant proteins SP-B and SP-C in BLES. Unlike the effect of Mini-B on oriented POPC-d_{31}/POPG bilayers, addition of 1 mol % Mini-B to oriented BLES lipid bilayers did not significantly increase the fraction of unoriented bilayer material. This means that the additional presence of 1 mol % Mini-B did not significantly increase the perturbation of bilayer orientation in oriented BLES. Surprisingly, however, the presence of 1 mol % SP-B_{CTERM} + SP-B_{NTERM} did have a strong effect on the fraction

of unoriented bilayer material in BLES. The spectrum shown in Figure 4.10C is for oriented BLES with 1 mol % SP-B_{CTERM} + SP-B_{NTERM}. Unlike its effect on oriented POPC-d_{31}/POPG bilayers, the presence of SP-B_{CTERM} + SP-B_{NTERM} in oriented BLES induced the formation of an unoriented fraction to a greater extent and also increased the orientational ordering of lipids in the oriented fraction in comparison to that of oriented bilayers with no added peptide.

Figure 4.11 shows the order parameter profiles for oriented BLES in the presence and absence of the SP-B peptides. The two order parameter values at carbon position two (C2) in DPPC-d_{62} indicate that the two deuterons on the C2 methylene of the *sn*-2 chain are not equivalent. Comparison of the order parameter profiles A and B in Figure 4.11 shows that addition of Mini-B to oriented BLES lipid bilayers does not significantly change the orientational order parameter profile of the lipid acyl chain. On the other hand addition of 1 mol % SP-B_{CTERM} + SP-B_{NTERM} did increase the orientational order of the lipids in oriented fraction of the BLES bilayers.

Figure 4.12 shows the ^{31}P spectra for oriented BLES with and without SP-B peptides. The spectrum shown in Figure 4.12A is for oriented BLES without peptide. It shows that the sample is well-oriented with only a small unoriented fraction. The peak at 36.8 ppm arises from the PC head group fraction and the peak at 32.1 ppm arises from the PG head group fraction. The ratio in peak intensity of the PC and PG lipids is consistent with the ratio of the PC and PG in the natural BLES surfactant mixture. The small intensity feature at -8.0 ppm might be due to the presence of a small unoriented fraction resulting from the presence of natural SP-B and natural SP-C in BLES. Addition of 1 mol % Mini-B to the oriented bilayers did not significantly increase the unoriented fraction, but instead slightly changed the head group conformation in the oriented fraction of lipids. As shown in the deuterium spectra of Figure 4.10, addition of 1 mol % SP-B_{CTERM} + SP-B_{NTERM} to oriented BLES lipid bilayers induced a greater fraction of unoriented bilayer material than Mini-B. The peak intensity at -7.7 ppm is a measure of how much unoriented bilayer material is formed in presence of 1 mol % SP-B_{CTERM} + SP-

B_{NTERM}. In contrast to its small effect on oriented POPC-d_{31}/POPG (7:3) lipid bilayers, SP-B_{CTERM} + SP-B_{NTERM} had a surprisingly strong effect on oriented BLES lipid bilayers.

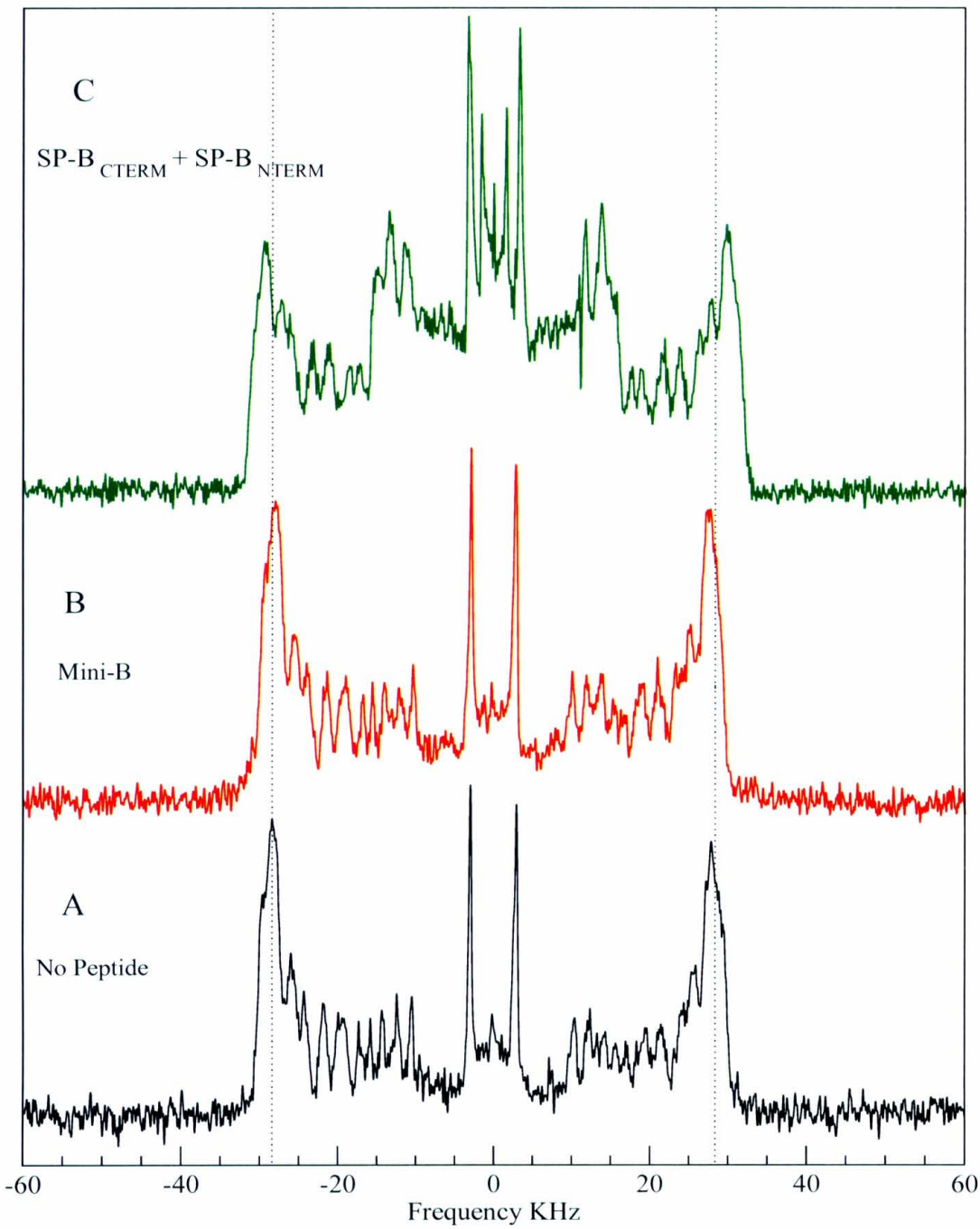

Figure 4.10: ^{2}H-NMR of (A) oriented BLES, (B) oriented BLES with 1 mol % Mini-B and (C) oriented BLES with 1 mol % SP-B $_{CTERM}$ + SP-B $_{NTERM}$.

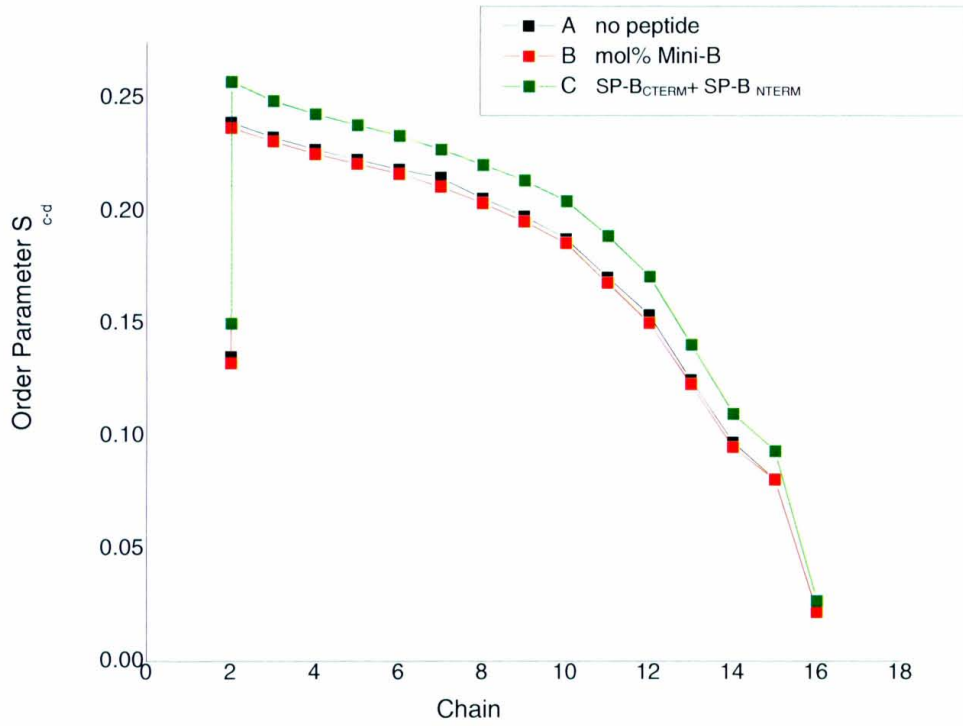

Figure 4.11: ^{2}H-NMR order parameter profiles of (A) oriented BLES, (B) oriented BLES with 1 mol % Mini-B and (C) oriented BLES with 1 mol % SP-B $_{CTERM}$ + SP-B $_{NTERM}$. (The deuterons at C2 positions of *sn*-2 chain of DPPC are not equivalent, thus have different orientational order parameter values (Davis 1983)). (Error bars are smaller than the symbol size).

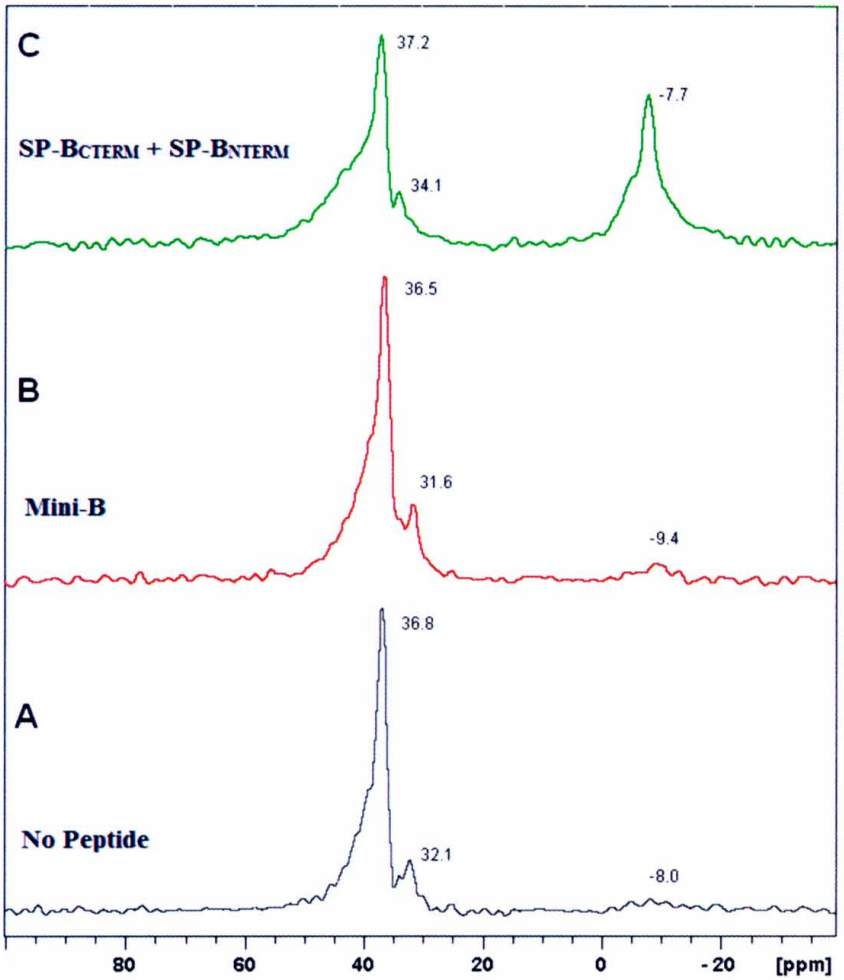

Figure 4.12: ^{31}P-NMR spectra of (A) oriented BLES, (B) oriented BLES with 1 mol % Mini-B, and (C) oriented BLES with 1 mol % SP-B $_{CTERM}$ + SP-B $_{NTERM}$

4.2 Multilamellar Vesicles (MLVs) Lipid bilayers

4.2.1 Multilamellar vesicle samples of POPC-d_{31}/POPG (7:3) with Mini-B and SP-B $_{CTERM}$ + SP-B $_{NTERM}$

In the next sequence of experiments, we used multilamellar vesicles (MLVs) to study the interactions of SP-B peptides with POPC-d_{31}/POPG bilayers and to separate SP-B peptide effects on chain order from their large length-scale perturbations of bilayer orientation. We studied these vesicles by incorporating 1 mol % Mini-B or 1 mol % SP-B_{CTERM} + SP-B_{NTERM} into the vesicle samples and using solid-state ^{2}H-NMR and ^{31}P-NMR.

The ^{2}H-NMR spectra in Figure 4.13 are for multilamellar vesicles composed of POPC-d_{31}/POPG (7:3) in the presence and absence of SP-B fragments. All spectra are characteristic of fast and axially symmetric chain reorientation in the liquid crystalline phase of the lipid bilayer. Multilamellar vesicles have large fractions of their lipids aligned perpendicular to the magnetic field and very small fractions of lipids oriented parallel to the direction of magnetic field. This is seen, in deuterium spectra, as the Pake-doublet shape with a more intense signal at the splitting corresponding to the bilayer normal oriented perpendicular to the magnetic field and a less intense signal at the splitting corresonding to the bilayer normal being oriented parallel to the magnetic field. Since the acyl chain of POPC-d_{31} in the lipid mixture was perdeuterated, the ^{2}H spectrum of the POPC-d_{31}/POPG (7:3) MLV sample is a superposition of Pake-doublets corresponding to each deuteron along the length of the 16-carbon the acyl chain.

The ^{2}H spectrum in Figure 4.13A is for peptide-free POPC-d_{31}/POPG (7:3) vesicles. Addition of 1 mol % Mini-B or 1 mol % SP-B_{CTERM} + SP-B_{NTERM} (Figure 4.13B and 4.13C) did not result in any significant change in the shape of the spectrum or any significant change in quadrupolar splitting.

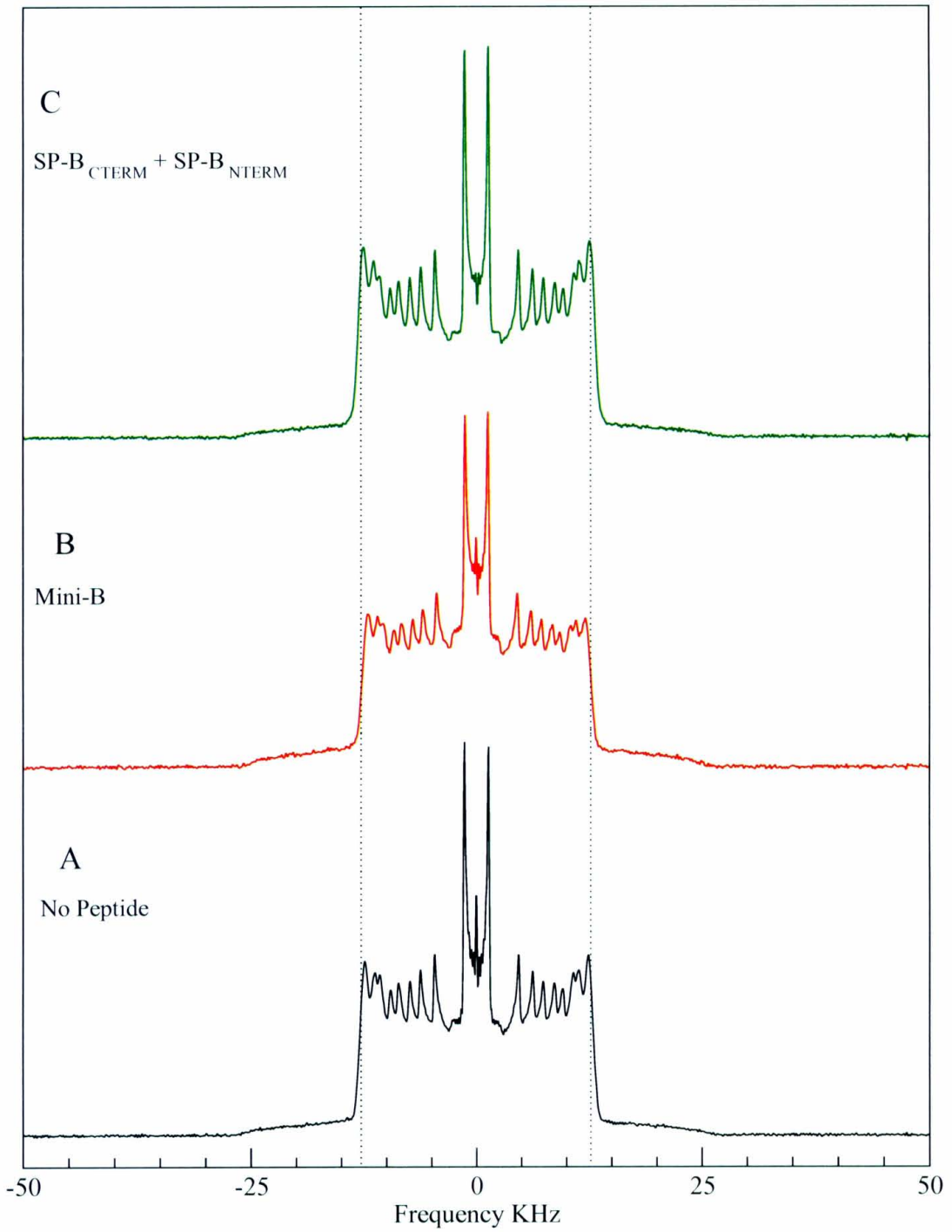

Figure 4.13: ^{2}H-NMR of vesicle (A) POPC-d_{31}/POPG, (B) POPC-d_{31}/POPG with 1 mol % Mini-B and (C) POPC-d_{31}/POPG with 1 mol % SP-B $_{CTERM}$ + SP-B $_{NTERM}$.

The spectra in Figure 4.14 are dePaked transforms of spectra in Figure 4.13. All spectra are dePaked to give spectra corresponding to a bilayer normal orientation parallel to the external magnetic field. The dePaked ^{2}H spectrum for the peptide-free vesicle sample, Figure 4.14A, is similar to the ^{2}H spectrum (Figure 4.7A) for the peptide-free oriented lipid bilayer with its bilayer normal parallel to the magnetic field. The dePaked spectra for vesicles containing 1 mol % Mini-B and 1 mol % SP-B $_{CTERM}$ + SP-B $_{NTERM}$ (Figure 4.13B and 4.13C) did not show any changes in shape of the spectra, relative to Figure 4.14A, but did show a small increase in the width of the deuterium peaks.

Figure 4.15 illustrates the smoothed orientational order parameter profiles obtained after dePaking the deuterium-NMR spectra of the vesicle samples. It shows that addition of 1 mol % Mini-B slightly reduced the chain orienational order in POPC-d_{31}/POPG (7:3) vesicle lipid bilayers, whereas addition of 1 mol % SP-B_{CTERM} + SP-B_{NTERM} slightly increased the chain orientational order in such vesicle lipid bilayers. The change in the average area per lipid of POPC-d_{31}/POPG (7:3) vesicle bilayers was not significantly different when 1 mol % of Mini-B or SP-B_{CTERM} + SP-B_{NTERM} was added. It is important to note that, unlike the oriented sample spectra, the vesicle spectra are not expected to be sensitive to large scale perturbation of local bilayer orientation such as would occur, for example, if the peptide induced the formation of bilayer protrusions.

Figure 4.16 shows ^{31}P spectra of vesicle samples composed of POPC-d_{31}/POPG (7:3) with and without peptide. The shapes of all ^{31}P spectra are characteristic of the liquid crystalline phase of lipid bilayers having a random distribution of bilayer normal directions. The high intensity at about -12 ppm arises from the lipids, in the vesicles, which have bilayer normals oriented perpendicular to the external magnetic field whereas the small intensity about at 25 ppm arises from lipids which have bilayer normals parallel to the magnetic field. The spectrum in Figure 4.16A is for a multilamellar vesicle sample composed of POPC-d_{31}/POPG (7:3). The feature at a chemical shift of -13.3 ppm is from the POPC head groups and the feature with a chemical shift of -10.8 ppm is from the

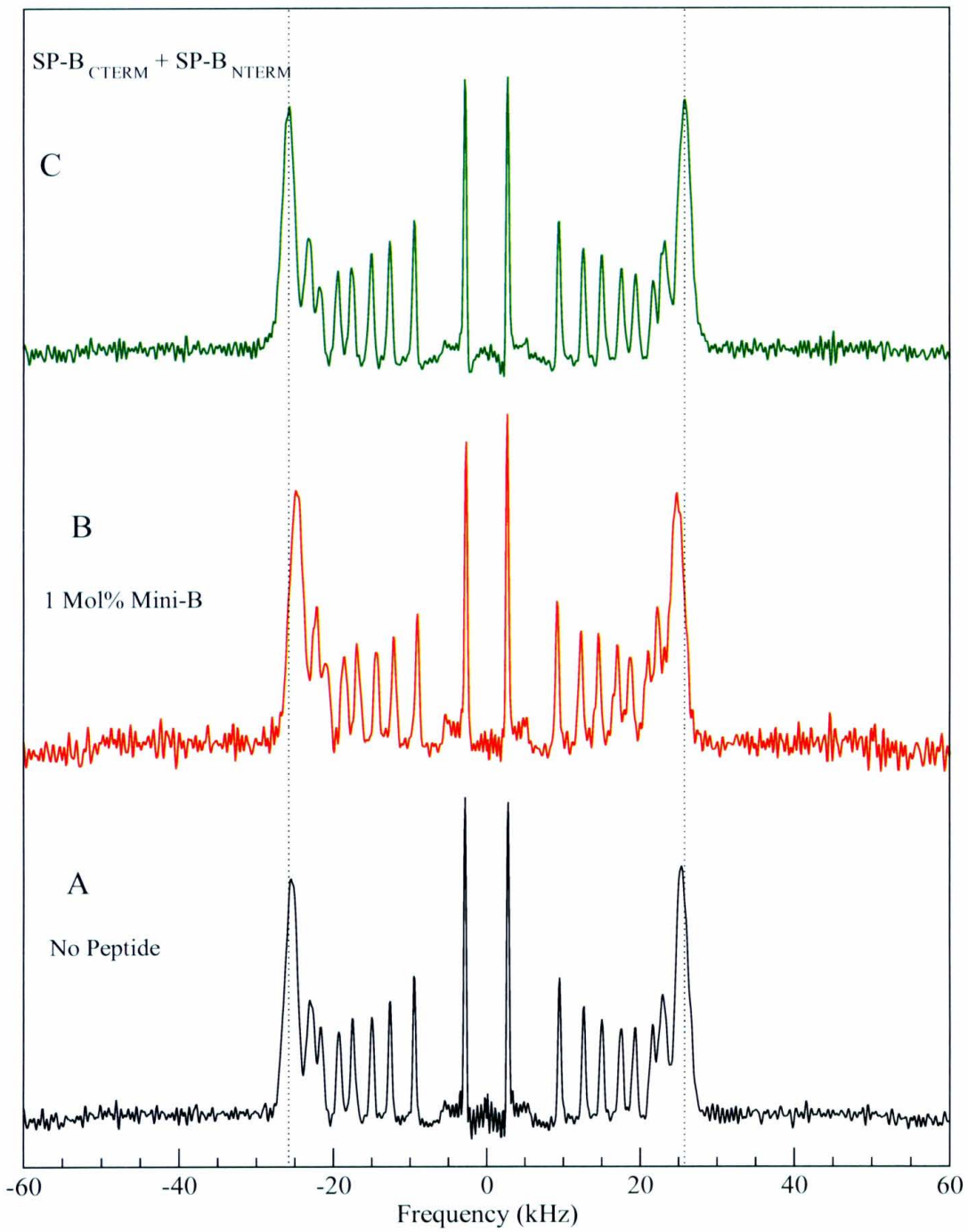

Figure 4.14: DePaked ^{2}H-NMR spectra of vesicle (A) POPC-d_{31}/POPG, (B) POPC-d_{31}/POPG with 1 mol % Mini-B and (C) POPC-d_{31}/POPG with 1 mol % SP-B $_{CTERM}$ + SP-B $_{NTERM}$.

POPG. The intensity ratio is similar to the ratio of PC and PG head group components in the mixture. Addition of 1 mol % Mini-B reduced the separation between PC and PG peaks, indicating a shift toward more similar orientations of these headgroups. Addition of Mini-B resulted in the chemical shift of the most prominent feature being slightly shifted upfield to -12.9 ppm possibly indicating a small change in head group conformation. However addition of 1 mol % SP-B_{CTERM} + SP-B_{NTERM} did appear to significantly change the head group orientation compared to Mini-B. In presence of 1 mol % SP-B_{CTERM} + SP-B_{NTERM} the chemical shift changed by 4.7 ppm in the downfield direction to -8.0 ppm.

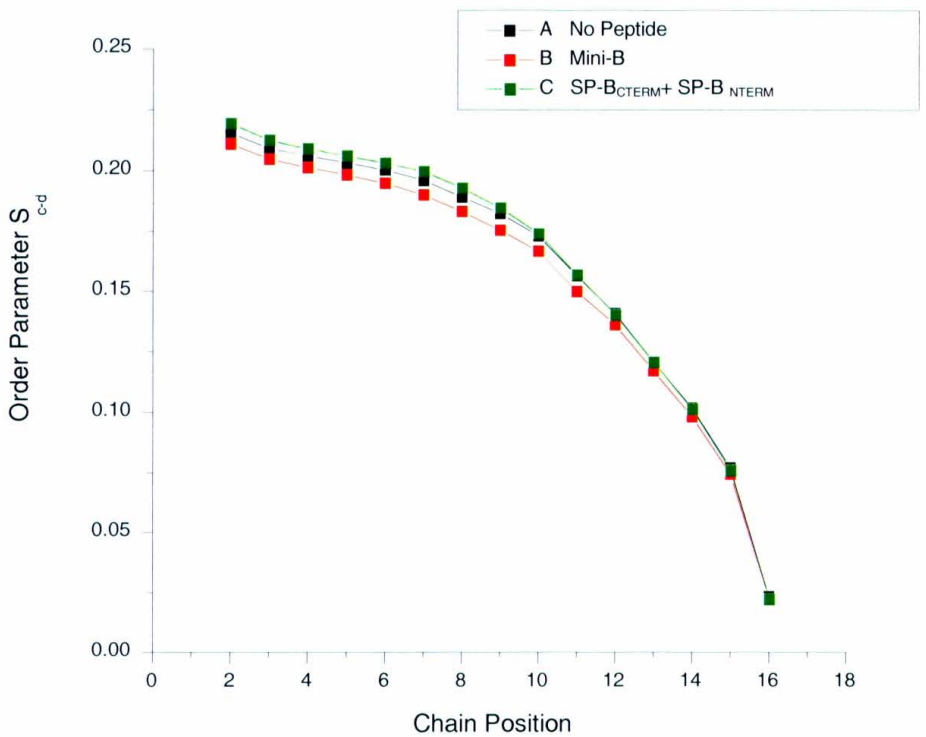

Figure 4.15: ^{2}H-NMR order parameter profiles of vesicle (A) POPC-d_{31}/POPG, (B) POPC-d_{31}/POPG with 1 mol% Mini-B and (C) POPC-d_{31}/POPG with 1 mol % SP-B $_{CTERM}$ + SP-B $_{NTERM}$. (Error bars are smaller than the symbol size).

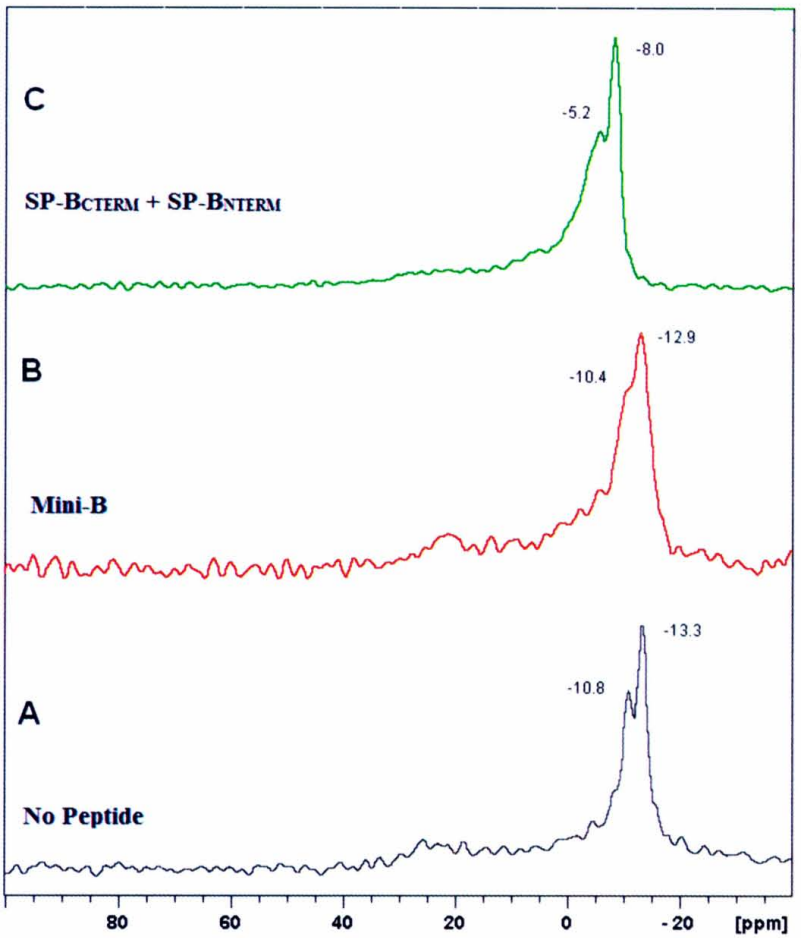

Figure 4.16: ^{31}P-NMR spectra of vesicle (A) POPC-d_{31}/POPG, (B) POPC-d_{31}/POPG with 1 mol % Mini-B and (C) POPC-d_{31}/POPG with 1 mol % SP-B $_{CTERM}$ + SP-B $_{NTERM}$.

4.2.2 Multilamellar vesicle samples of BLES with Mini-B and SP-B$_{CTERM}$ + SP-B$_{NTERM}$

Multilamellar vesicle bilayers composed of BLES were prepared to study the lipid-peptide interactions in natural surfactant extract and to compare with the results from model vesicle bilayers composed of POPC-d_{31}/POPG (7:3).

Figure 4.17 shows deuterium-NMR spectra of the BLES vesicles both in the absence and presence of peptide. The spectra show poor signal to noise ratio due to the incorporation of only 2.5% DPPC-d_{62} into the BLES vesicles. The spectrum in Figure 4.17A is for BLES vesicles without peptide and is characteristic of fast and axially symmetric motion of lipids in the bilayer. Addition of 1 mol % Mini-B and 1 mol % SP-B_{CTERM} + SP-B_{NTERM} did not change the quadrupolar splitting but did introduce a narrow central peak characteristic of isotropic reorientation, suggesting the formation of either micelles or rapidly tumbling small vesicles. This observation suggests that, in the presence of 1 mol % SP-B peptides, a small fraction of the sample separates into small vesicles or micelles. Due to the poor signal-to-noise ratio, ^{2}H spectra could not be dePaked; thus, no order parameter profiles were calculated.

Figure 4.18 shows ^{31}P spectra for BLES vesicles with and without peptide. The spectrum in Figure 4.18A is for a vesicle sample with no peptide and shows a feature with a chemical shift of -14.6 ppm, corresponding to the PC head group, and a feature with a chemical shift of -11.5 ppm, corresponding to the PG head group. The intensities are consistent with relative PC and PG concentrations in BLES. The spectrum in Figure 4.18A shows that addition of 1 mol % Mini-B to BLES, introduced a feature with a chemical shift of 0.7 ppm, corresponding to an anisotropically reorienting fraction, and changed the chemical shifts of the PC and PG head groups towards the downfield direction. Isotropic chemical shift is a direct indication of the presence of fast tumbling structures such as micelles and small vesicle formations. In the presence of Mini-B, the PC and PG peaks are very well resolved, suggesting that Mini-B introduced different orientations of the PC and PG headgroups that were more distinct in the presence of Mini-B than in the peptide-free vesicles. The chemical shifts changed from -14.6 ppm to -12.5 ppm and from -11.5 ppm to -7.8 ppm for PC and PG components, respectively, in presence of Mini-B. The effects of 1 mol % SP-B_{CTERM} + SP-B_{NTERM} on the PC and PG ^{31}P chemical shift was smaller in comparison to those induced by 1 mol % Mini-B.

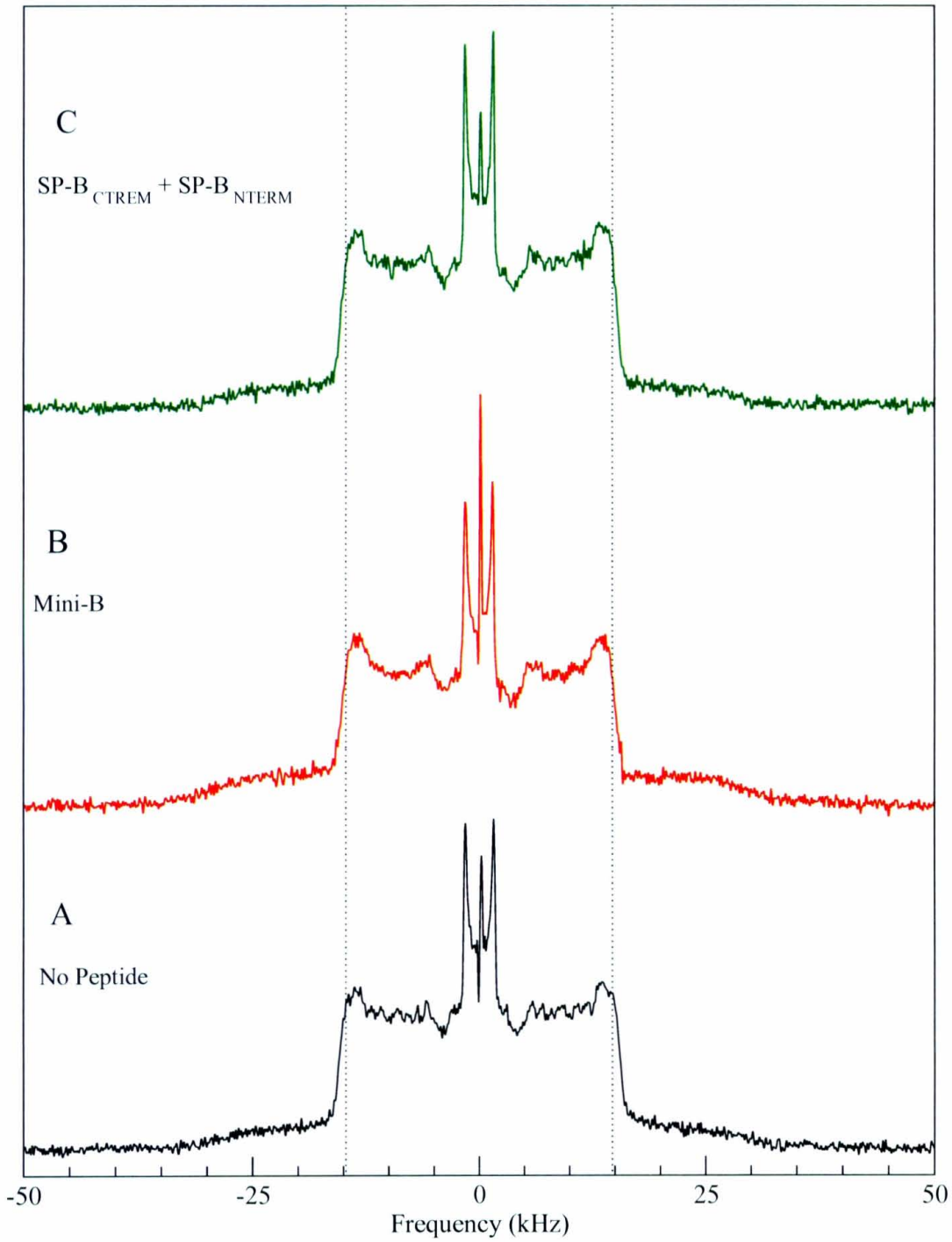

Figure 4.17: ^{2}H-NMR spectra of (A) oriented BLES, (B) oriented BLES with 1 mol % Mini-B and (C) oriented BLES with 1 mol % SP-B $_{CTERM}$ + SP-B $_{NTERM}$.

In the presence of SP-B_{CTERM} + SP-B_{NTERM}, the ^{31}P spectrum shows a small feature at 1.1 ppm presumably corresponding to a small isotropically-reorienting fraction of the sample. The chemical shift values are changed by 1.4 ppm to -13.2 ppm and by 2.2 ppm to -9.3 ppm for PC and PG, respectively.

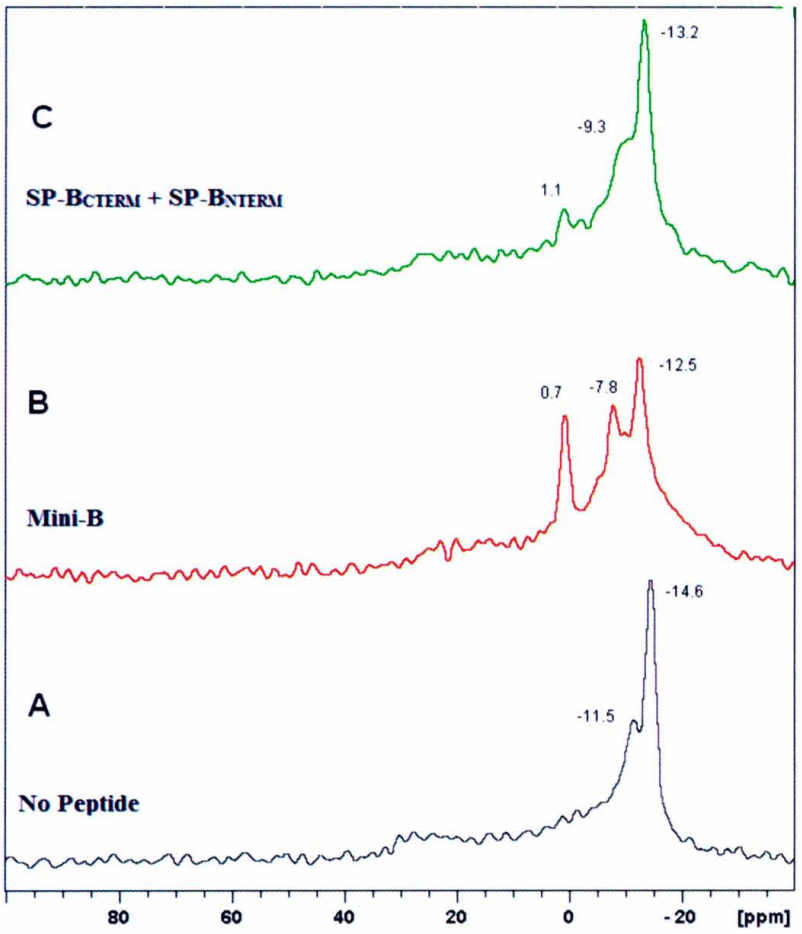

Figure 4.18: ^{31}P-NMR spectra of vesicle (A) BLES, (B) BLES with 1 mol % Mini-B and (C) BLES with 1 mol % SP-B $_{CTERM}$ + SP-B $_{NTERM}$.

4.3 Tubular Myelin reconstruction

It is known that Tubular Myelin (TM) can be prepared in vitro with a specific combination of lung surfactant lipids, DPPC and egg PG, and proteins SP-A and SP-B in presence of calcium (Suzuki et al. 1989, Williams et al. 1991). In surfactant deficient rat models, Mini-B showed significant biological activity (oxygen levels in blood and lung compliance) as effective as full length SP-B (Waring et al. 2005). In order to learn if Mini-B can support the formation of tubular myelin, samples containing all of the TM components were prepared with either SP-B or Mini-B. Figure 4.19 shows the formation of tubular myelin with DPPC/egg PG (7:3), SP-A and SP-B. The structures seen in Figure 4.19 look like typical lattice-like structures and elongated tubes which are characteristic of tubular myelin structures. As seen in Figure 4.20, the lattice-like structures were not observed when SP-B was replaced by Mini-B at the same molar ratio. In presence of Mini-B, the electron micrographs do not contain any rectangular cross-sectional structures like those seen in the sample with SP-B. Instead there are mostly lamellar bodies and few long tubules as shown in Figure 4.20.

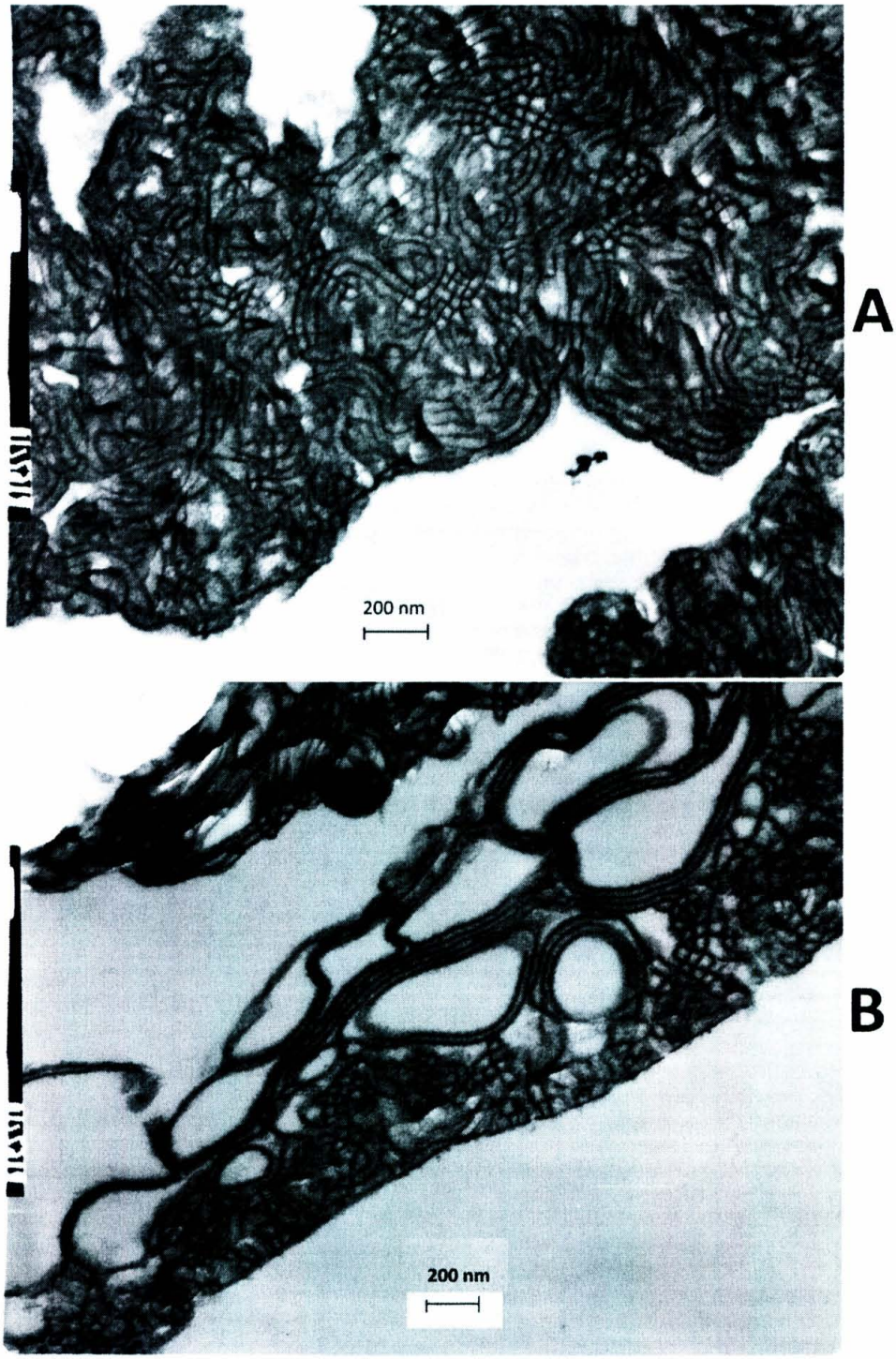

Figure 4.19: Representative Electron Micrographs showing tubular myelin structures formed in mixture of DPPC, egg PG, SP-A and SP-B.

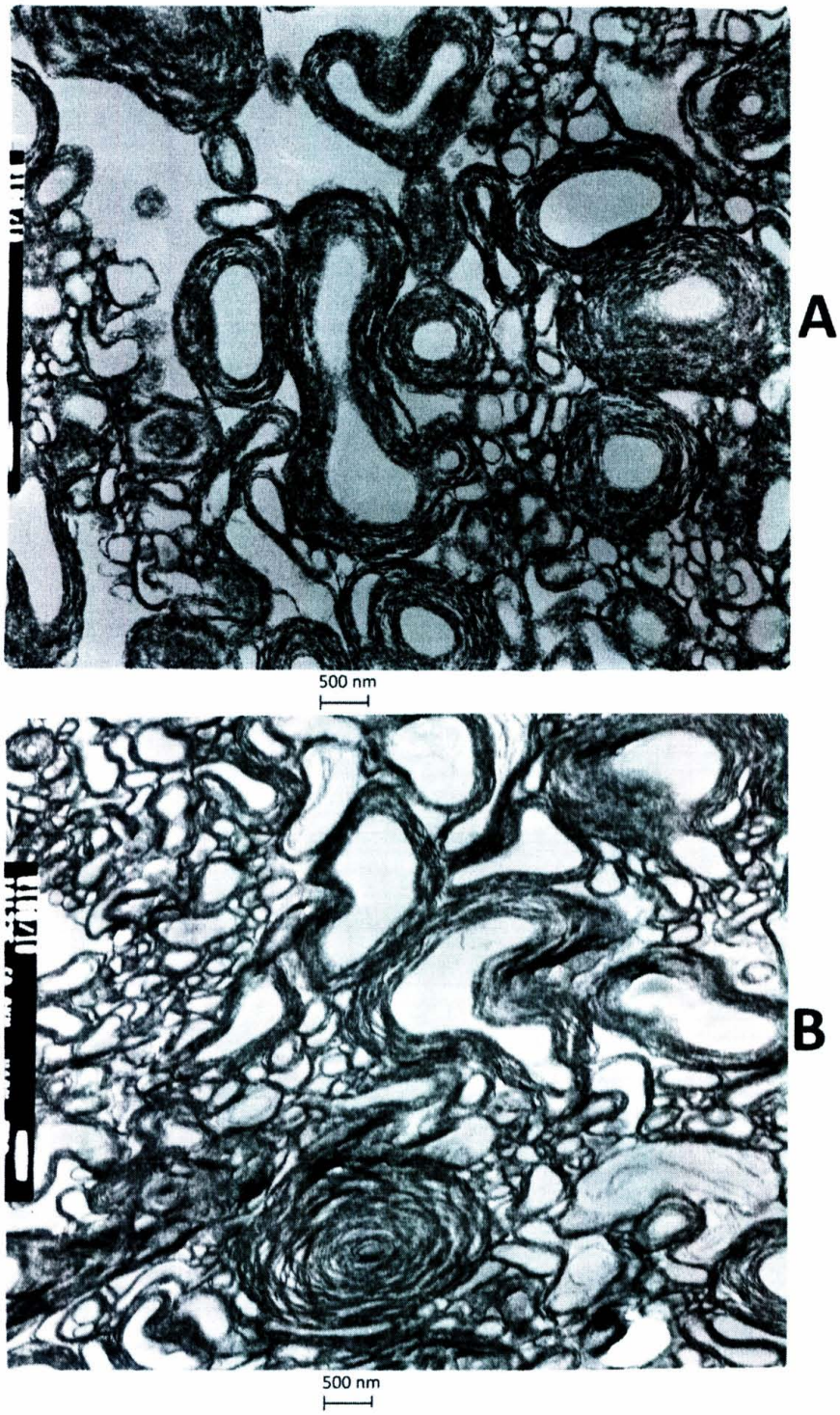

Figure 4.20: Representative Electron Micrograph showing non tubular myelin structures formed in mixture of DPPC, egg PG, SP-A and Mini-B.

Chapter 5

Discussion and conclusions

SP-B is essential for reducing surface tension at the alveolar air-water interface and thus for the function of the lung surfactant system (Whitsett et al. 1995 and Clark et al. 1995). At least part of this essential function likely relates to SP-B's contribution to surfactant layer maintenance and renewal through facilitating the contact and transfer of surfactant material between the surface layer and adjacent bilayer reservoirs (Perez-Gil 2008). Currently, the structure of full length SP-B has not yet been determined, but some fragments, including SP-B_{CTERM}, SP-B_{NTERM} and Mini-B, do have experimental structures (Sarker et al. 2007, Booth et al. 2004 and Kurutz and Lee et al. 2002). The structure of Mini-B is shown in Figure 1.5. The amino acid sequence homology indicates that SP-B belongs to the Saposin superfamily (Munford et al. 1995). SP-B is presumed to contain four to five helices and a large fraction of hydrophobic residues which presumably facilitate its strong association with lipids. One suggestion is that SP-B orients in bilayers in such a way that peptide helices are parallel to the bilayer surface and that the hydrophobic region of SP-B inserts into the hydrophobic bilayer interface (Vandenbussche et al. 1992). N-terminal and C-terminal fragments of SP-B, SP-B_{CTERM} and SP-B_{NTERM}, possess significant biological activity, either individually or when linked together in the form of Min-B. In surfactant-deficient rats, Mini-B was found to support oxygenation levels in blood as well as SP-B does (Waring et al. 2005, Walther et al. 2010).

A number of biophysical studies have been performed with fragments of SP-B (e.g. Perez-Gil 2008, Dico et al. 1997, Yang et al. 2009, Russell-Schulz et al. 2009, Morrow et al. 2004, Antharam et al. 2008, Farver et al. 2010). Understanding of how these peptide fragments modify lipid organization will help us to understand the functional mechanism of full length SP-B. Such studies have shown that SP-B and fragments can modify lipid organization and induce slight changes in chain orientational order in surfactant lipid multilamellar bilayer dispersions (Russell-Schulz et al. 2009, Dico et al. 1997). Recent studies of the SP-B fragment, SP-B_{CTERM}, in mechanically oriented bilayers of POPC, POPG, POPC/POPG, and BLES (Yang et al. 2009, Bertani et al. 2012) showed that, in addition to a small perturbation of lipid chain orientational

order, it also induced the formation of unoriented bilayer regions that were large enough to preclude averaging by exchange with the oriented bilayer fraction.

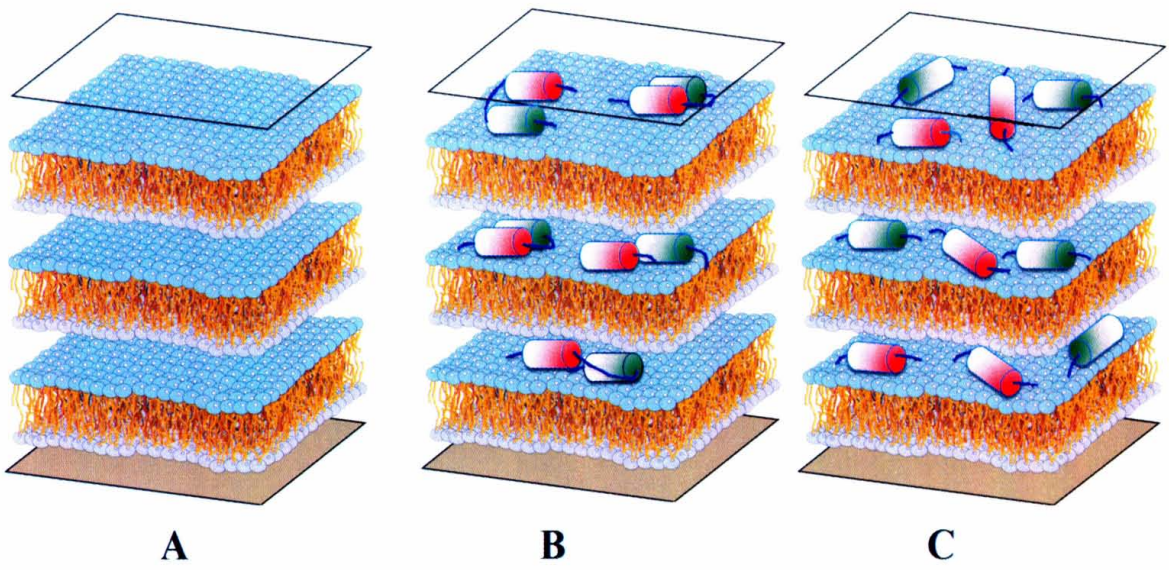

Figure 5.1: Cartoon representations of A) oriented bilayers with no peptide, B) oriented bilayers with Mini-B, and C) oriented bilayers with SP-B_{CTERM} and SP-B_{NTERM} separately.

The current study is focused on the effects of Mini-B or SP-B_{CTERM} + SP-B_{NTERM} (see Figure 5.1) on model and natural lung surfactant bilayers and these experiments were carried out using solid-state ^{2}H- and ^{31}P-NMR spectroscopy. Our aim was to work at concentrations and conditions that are relevant to physiological conditions (temperature, peptide concentration and lipid mixture) of lung surfactant. Thus the experiments were carried out at near physiological conditions, with 1 mol % peptide and temperatures of 23 and 35 ^{o}C for POPC/POPG and BLES respectively, which are close to physiological conditions for BLES and above the liquid-crystalline transition temperature for model lipid system. In general, in bovine surfactant, SP-B accounts only for about 0.5% of the surfactant dry weight which is about 4200 phospholipids per SP-B dimer (Zuo et al. 2008). The peptide fractions of 1 mol % used in our work correspond to about 5% by dry

sample weight which is slightly higher than physiological levels. The concentrations used in earlier studies of full length SP-B or fragments were much higher (up to 17% wt/wt) compared to the 1 mol % levels in our work. Therefore, this work with more physiologically relevant conditions complements earlier model studies.

A major focus of my research was to examine the effect of the peptides on bilayer properties over large length scales. These effects were monitored by observing the changes in NMR spectra of lipids with addition of peptide. Our studies show that SP-B fragments perturbed the bilayer orientation in mechanically oriented bilayers and induced an unoriented fraction of lipids. These perturbations were on scales that were large enough to preclude averaging by exchange with the oriented bilayer fraction. Mini-B has a more pronounced effect on model POPC/POPG oriented bilayers in comparison to SP-B_{CTERM} + SP-B_{NTERM} (Figure 4.7 B and C). In contrast, SP-B_{CTERM}+ SP-B_{NTERM} has a greater effect on natural BLES oriented bilayers than Mini-B (Figure 10 B, C). Surprisingly Mini-B did not significantly affect BLES oriented bilayers (Figure 4.10 B). Similarly, SP-B_{CTERM} + SP-B_{NTERM} did not significantly affect oriented POPC-d_{31}/POPG bilayers (Figure 4.7 C). We are not yet able to explain this difference. Nevertheless, this comparison suggests that the degree of peptide-induced unorientation is sensitive to the lipid bilayer composition, including the degree of lipid chain saturation, the presence of native hydrophobic protein, and the peptide structure.

In addition to disrupting bilayer orientation on large scales, SP-B fragments also slightly affected the orientational order of lipid chains in the fractions of the lipids that remained oriented (Figure 4.8 and Figure 4.11). The peptides also increased mosaic spread, the broadening of the distribution of bilayer normal directions about the average normal orientation. Changes in the deuterium orientational order parameter profiles are similar to previous studies showing that SP-B fragments composed of either N-terminal helix or C-terminal helix can induce slight changes in chain orientational order in surfactant lipid bilayers (Yang et al. 2009, Russell- Schulz et al. 2009).

The ^{31}P-NMR spectra of oriented bilayers, which indicate effects on the phospholipid headgroups, complement observations obtained from ^{2}H-NMR of the acyl chains discussed above. SP-B_{CTERM} + SP-B_{NTERM} in oriented BLES bilayers induced a considerable fraction of the lipids to lose their orientation. The unoriented structures must be large enough to preclude averaging by exchange with the oriented bilayer fraction on NMR time scale (Figure 4.12 C). Mini-B and SP-B_{CTERM} + SP-B_{NTERM} did not show significant effects on the orientation of oriented BLES and POPC-d_{31}/POPG (Figure 4.12 B and Figure 4.9 B). However, the presence of these SP-B peptides in oriented bilayers increased mosaic spread, as observed by the increased width of the peak in ^{31}P-NMR spectra.

In addition to oriented lipid bilayers, subsequent studies with multilamellar vesicles (MLVs) were also performed with SP-B fragments Mini-B or SP-B_{CTERM}+ SP-B_{NTERM} in model and natural surfactant multilamellar vesicle (MLV) systems. Comparison of spectra from mechanically oriented samples and vesicles can separate changes in chain orientational order parameter from large length-scale perturbations of bilayer orientations. ^{2}H-NMR and ^{31}P-NMR spectra showed slight changes in lipid chain orientational order.

It may be helpful to consider how the peptide-induced perturbations in bilayer orientation observed herein may arise. The oriented samples were prepared by deposition of the lipid or lipid-peptide solution on mica plates followed by drying, hydration, and stacking of the mica plates. The peptide-free samples which are well oriented may be better aligned during the hydration stage or more easily oriented upon stacking of the mica plates. In the presence of Mini-B or SP-B_{CTERM} + SP-B_{NTERM}, the misalignment or departures from average orientation in mica-supported bilayers might take place either during hydration of the sample, prior to the stacking, or after stacking the mica plates. Regardless of whether the effect of the peptide is primarily felt at the stacking stage or at both the hydration and stacking stages of the alignment process, the resulting misalignment might be considered to amount to the introduction of defects into planar bilayer stacks. One way to imagine this happening would be if peptide-induced coupling

of adjacent bilayers at the hydration stage were to promote the persistence of protrusions and/or large scale bilayer corrugations (10-100 μs) which could then be trapped when the bilayers were more confined in the stack of mica plates. Possible mechanisms for such coupling might include direct linking of adjacent bilayers by shared peptides or the bridging of adjacent bilayers by peptide-stabilized stalk structures.

The peptide-induced disruptions in bilayer orientation observed here may indicate a molecular mechanism of full length SP-B. SP-B is known to promote rapid transfer of surfactant to the air water interface as required for lung function. Proper functioning and maintenance of lung surfactant requires the recruitment and rapid transfer of surfactant material between the surface active layer and adjacent bilayer reservoirs (Possmayer et al. 2010, Frey et al. 2010). SP-B has been suggested to induce bilayer folding from the monolayer at the air-water interface, as illustrated in recent molecular dynamics simulations (Baoukina and Tieleman et al. 2011). The multilayer structures of lung surfactant imply a need for close contacts between bilayers and the surface active monolayer layer. It is thought SP-B might promote highly curved stalk structures which facilitate the lipid transfer between surface active layer and surfactant reservoirs. This might reflect the stabilization of protrusions of peptide linking of adjacent bilayers by peptide-induced stalks. Such models of SP-B mechanism are consistent with the SP-B peptide-induced promotion of unoriented bilayer structures observed in this study.

The ^{2}H-NMR and ^{31}P-NMR studies were one approach to study the effect of SP-B peptides on large scale lipid orientation. An alternative means of probing Mini-B's effect on large-scale lipid structures was presented in the tubular myelin (TM) studies. Tubular myelin structures such as square lattices and elongated tubules have been observed via microscopy in presence of both SP-B and SP-A (Suzuki et al. 1989, Williams et al. 1991). Both SP-A and SP-B are required for the formation of tubular myelin. In our studies, we also observed similar type of lipid structures with SP-B and SP-A. However, when Mini-B replaced SP-B, no such structures were found, as shown in Figure 4.20. Mini-B has been shown to be just as effective as SP-B at improve blood oxygenation in surfactant deficient rodents (Waring et al. 2005, Walther et al. 2010). Therefore, the fact

that it does not support the structural formation of tubular myelin-like structures in the presence of SP-A, indicates that TM structures may not be important in exogenously added surfactant. Genetically modified mice lacking SP-A apparently showed normal lung function (Korfhagen et al. 1996), suggesting that mice lacking the tubular myelin structure can still have normal lung function. So, tubular myelin formation may not be prerequisite for the function of lung surfactant and Mini-B does not contain the key domains which enable tubular myelin formation.

References:

Antharam VC, Farver RS, Kuznetsova A, Sippel, KH, Mills FD, Elliott DW, Sternin E, Long JR (2008). Interactions of the C-terminus of lung surfactant protein B with lipid bilayers are modulated by acyl chain saturation. Biochim Biophys Acta; 1778, 2544-2554.

Baatz JE, Elledge B, Whitsett JA (1990). Surfactant protein SP-B induces lipid ordering at the surface of model membranes bilayers. Biochemistry; 29(28), 6714-6720.

Bertani P, Vidovic V, Yang TC (2012). Orientation and depth of surfactant protein B C-terminal helix in lung surfactant bilayers. Biochim Biophys Acta; 1818(5), 1165-72.

Bligh E, Dyer W (1959). A rapid method of total lipid extraction and purification. Can J Biochem Phys; 37, 911–917.

Bloom M, Davis JH, MacKay AL (1981). Direct determination of the oriented sample NMR spectrum from the powder spectrum for systems with local axial symmetry. Chem Phys Lett; 80, 198 –202.

Bloom M, Evans E, Mourisen OG (1991). Properties of the fluid lipid-bilayer component of cell membranes: a perspective. Q Rev BioPhys; 24(3), 293-397.

Booth V, Waring AJ, Walther FJ, Keough KM (2004). NMR structures of the C-terminal segment of surfactant protein B in detergent micelles and hexafluoro-2-propanol. Biochemistry; 43, 15187-15194.

Burnett LJ and Muller BH (1971). Deuteron quadrupole coupling constants in three solid deuterated paraffin hydrocarbons: C2D6, C4D10, C6D14. J Chem Phys; 55, 5829–5831.

Clark JC, Wert SE, Bachurski CJ, Stahlman MT, Stripp BR, Weaver TE, Whitsett JA (1995). Targeted disruption of the surfactant protein B gene disrupts surfactant homeostasis, causing respiratory failure in newborn mice. Proc Natl Acad Sci U S A; 92, 7794-7798

Clements J (1957). Surface tensions of lung extracts. Proc Soc Exp Biol Med; 95, 170-172.

Crewels L, Van Golde LM, and Haagsman HP (1997). Review: The pulmonary surfactant system: biochemical and clinical aspects. Lung; 175(1), 1-39.

Cruz A, Worthman LA, Serrano AG, Casals C, Keough KM, Pérez-Gil J (2000). Microstructure and dynamic surface properties of surfactant protein SP-B/ dipalmitoylphosphatidylcholine interfacial films spread from lipid–protein bilayers. Eur Biophys J; 29, 204–213.

Davis J H (1983). The description of membrane lipid conformation, order and dynamics by 2H-NMR. Biochim Biophys Acta; 737, 117-I71.

Davis J H, Jeffrey KR, Bloom M, Valic MI, Higgs TP (1976). Quadrupoleecho deuteron magnetic resonance spectroscopy in ordered hydrocarbon chains. Chem Phy Lett; 42(2), 390-394.

Dico AS, Hancock J, Morrow MR, Stewart J, Harris S, Keough KM (1997). Pulmonary surfactant protein SP-B interacts similarly with dipalmitoylphosphatidylglycerol and dipalmitoylphosphatidylcholine in phosphatidylcholine/phosphatidylglycerol mixtures. Biochemistry; 36, 4172-4177.

Farver RS, Mills FD, Antharam VC, Chebukati JN, Fanucci GE, Long JR (2010). Lipid Polymorphism Induced by Surfactant Peptide SP-B1-25. Biophy J; 99(6), 773-1782.

Frey SL, Pocivavsek L, Waring AJ (2010). Functional importance of the NH2-terminal insertion sequence of lung surfactant protein B. Am J Physiol Lung Cell Mol Physiol; 298, L335-L347.

Gordon LM, Lee KY, Lipp MM, Zasadzinski JA, Walther FJ, Sherman MA, Waring AJ (2000). Conformational mapping of the N-terminal segment of surfactant protein B in lipid using 13C-enhanced Fourier transform infrared spectroscopy. J Pept Res; 55, 330–347.

Gunther A, Ruppert C, Schmidt R, Markart P, Grimminger F, Walmrath D, Seeger W (2001). Surfactant alteration and replacement in acute respiratory distress syndrome. Respir Res; 2(6), 353-64.

Hawgood S, Derrick M, Poulain F (1998). Structure and properties of surfactant protein B. Biochim Biophys Acta; 1408, 150-160.

Hawkins CA, Alba E and Tjandra N (2005). Solution structure of human saposin C in adetergent environment. J Mol Biol; 346, 1381-1392.

Ikegami M, Korfhagen TR, Whitsett JA, Bruno MD, Wert SE, Wada K, Jobe AH (1998). Characteristics of surfactant from SP-A-deficient mice. Am J Physiol; 275, L247-L254.

Johansson J, Curstedt T, Robertson B (1994). The proteins of the surfactant system. Europ Respir J; 7(2), 372-391.

King RJ, Klass DJ, Gikas EG, Clements JA (1973). Isolation of apoproteins from canine surface active material. Am J Physiol; 224, 788-795.

Korfhagen TR, Bruno MD, Ross GF, Huelsman KM, Ikegami M, Jobe AH, Wert SE, Stripp BR, Morris RE, Glasser SW, Bachurski CJ, Iwamoto HS, Whitsett JA (1996).

Altered surfactant function and structure in SP-A gene targeted mice. Proc Natl Acad Sci U S A; 93(18), 9594-9599.

Kurutz JW, Lee KY (2002). NMR structure of lung surfactant peptide SP-B (11-25). Biochemistry; 41, 9627-9636.

Lafleur M, Fine B, Sternin E, Cullis P R, Bloom M (1989). Smoothed orientational order profile of lipid bilayers by 2H-nuclear magnetic resonance. Biophys J; 56(5), 1037–1041.

Lang CJ, Postle AD, Orgeig S, Possmayer F, Bernhard W, Panda AK, Jurgens KD, Milsom WK, Nag K and Daniels CB (2005). Dipalmitoylphosphatidylcholine is not the major surfactant phospholipid species in all mammals. Am J Physiol-Reg I; 289, 1426-1439.

Liepinsh E, Andersson M, Ruysschaert JM and Otting G (1997). Saposin fold revealed by the NMR structure of NK-Lysin. Nat Struct Biol; 4, 793-795.

Lindhout DA, Thiessen A, Schieve D, and Sykes BD (2003). High-yield expression of isotopically labeled peptides for use in NMR studies. Protein Sci; 12, 1786-1791.

Lumb RH (1989). Phospholipid transfer proteins in mammalian lung. Am J Physiol; 257, L190-L194.

Lynch RG (2004). Surfactant and RDS in premature infants. FASEB J; 18, 1624.

Morrow MR, Abu-Libdeh N, Stewart J, Keough KM (2003). Interaction of Pulmonary Surfactant Protein SP-A with DPPC/Egg-PG Bilayers. Biophy J; 85, 2397–2405.

Morrow MR, Stewart J, Taneva S, Dico A, Keough KMW (2004). Perturbation of DPPC bilayers by high concentrations of pulmonary surfactant SP-B. Eur Biophy J; 33, 285-290.

Munford R S, Sheppard P O and O'Hara P J (1995). Saposin-like proteins (SAPLIP) carry out diverse functions on a common backbone structure. J Lipid Res; 36, 1653-1663.

Nag K, Keough KM and Morrow MR (2006). Probing perturbation of bovine lung surfactant extracts by albumin using DSC and 2H-NMR. Biophy J; 90, 3632–3642.

Nag K, Munro JG, Inchley K, Schürch S, Petersen NO, Possmayer F (1999). SP-B refining of pulmonary surfactant phospholipid films. Am J Physiol; 277, L1179–L1189.

Notter, Robert H. (2000). Lung surfactants: basic science and clinical applications. Crc Press Llc, New York.

Orgeig S, Daniels CB and Sullivan LC (2004). The development of the pulmonary surfactant system In: The Lung: Development, Aging and the Environment, edited by Harding R, Pinkerton K and Plopper C. London: Academic Press; 149-167.

Pastrana-Rios B, Flach CR, Brauner JW, Mautone AJ, and Mendelsohn R (1994). A Direct Test of the "Squeeze-Out" Hypothesis of Lung Surfactant g Surfactant Function. External Reflection FTIR at the Air/Water Interface. Biochemistry; 33, 5121-5127.

Pattle R (1955). Properties, function and origin of the alveolar lining layer, Nature; 175, 1125-1126.

Perez-Gil J (1993). Solubility of hydrophobic surfactant proteins in organic solvent/water mixtures: structural studies on SP-B and SP-C in aqueous organic solvents and lipids. Biochim Biophys Acta; 1168, 261–270.

Perez-Gil J (2008). Structure of pulmonary surfactant membranes and films: the role of proteins and lipid-protein interactions. Biochim Biophys Acta; 1778(7-8), 1676-1695.

Perez-Gil J, Casals C, Marsh D (1995). Interactions of hydrophobic lung surfactant proteins SP-B and SP-C with dipalmitoylphosphatidylcholine and dipalmitoylphosphatidylglycerol bilayers studied by electron spin resonance spectroscopy. Biochemistry; 34(12), 3964-3971.

Perez-Gil J, Weaver TE (2010). Pulmonary surfactant pathophysiology: current models and open questions. Physiology; 25,132-141.

Possmayer F (1997). Physicochemical aspects of pulmonary surfactant. In: Fetal and Neonatal Physiology, WB Saunders Company; 1259-1275.

Possmayer F, Hall SB, Haller T (2010). Recent advances in alveolar biology: some new looks at the alveolar interface. Resp Physiol Neurobi; 173, 55-64.

Rainey J K, Sykes B D (2005). Optimizing oriented planar-supported lipid samples for solid-state protein NMR. Biophy J; 89(4), 2792-2805.

Rooney SA (1998). Lung surfactant: cellular and molecular processing. Edited by Rooney SA. Austin, Texas. R. G. Landes Company.

Russell-Schulz B, Booth V, Morrow MR (2009). Perturbation of DPPC/POPG bilayers by the N-terminal helix of lung surfactant protein SP-B: a (2) H NMR study. Eur Biophy J; 38, 613-624.

Sarker M, Waring AJ, Walther FJ, Keough KM, Booth V (2007). Structure of mini-B, a functional fragment of surfactant protein B, in detergent micelles. Biochemistry; 46, 11047-11056.

Schurch S, Qanbar R, Bachofen H, Possmayer F (1995). The surface-associated surfactant reservoir in the alveolar lining. Biol. Neonate; 67, 61–76.

Seelig J (1977). Deutetium magnetic resonance: theory and applications to lipid membranes. Q Rev Biophys; 10(3), 353-418.

Seelig A and Seelig J (1974). The dynamic structure of fatty acyl chains in a phospholipid bilayer measured by deuterium magnetic resonance. Biochemistry; 13(23), 4839-4845.

Seelig J (1978). 31P nuclear magnetic resonance and the head group structure of phospholipids in membranes. Biochim Biophys Acta; 515(2), 105-140.

Serrano AG, Pérez-Gil J (2006). Protein-lipid interactions and surface activity in the pulmonary surfactant system. Chem Phys Lipids; 141, 105-118.

Smith I.C.P. and Ekiel, I.H. (1984). Phosphorus-31 NMR of phospholipids in membranes. In: Phosphorus-31 NMR: Principles and applications. D. Gorenstein, ed. Academic Press Inc. London, England; 447-475.

Sternin E, Bloom M, MacKay AL (1983). De-Pake-ing of NMR spectra. J Magn Reson 55, 274 –282.

Sternin E, Fine B, Bloom M, Tilcock CP, Wong KF (1988). Acyl chain orientational order in the hexagonal HII phase of phospholipid-water dispersions. Biophy J; 54, 689–694.

Suzuki Y, Fujita Y, Kogishi K (1989). Reconstruction of tubular myelin from synthetic lipids and proteins associated with pig pulmonary surfactant. Am Rev Respir dis; 140, 75-81.

Takamoto DY, Lipp MM, Von Nahmen A, Lee KY, Waring AJ and Zasadzinski JA (2001). Interaction of lung surfactant proteins with anionic phospholipids. Biophy J; 81, 153–169.

Vandenbussche G, Clercx A, Clercx M, Curstedt T, Johansson J, Jornvall H, Ruysschaert JM (1992). Secondary structure and orientation of the surfactant protein SP-B in a lipid environment. A Fourier transform infrared spectroscopy study. Biochemistry; 31 (38), 9169–9176.

Veldhuizen R, Nag K, Orgeig S and Possmayer F (1998). The role of lipids in pulmonary surfactant. Biochim Biophys Acta; 140 (8), 90-108.

Voorhout WF, Veenendaal T, Haagsman HP, Verkleij AJ, van Golde LM, Geuze HJ (1991). Surfactant protein A is localized at the corners of the pulmonary tubular myelin lattice. J Histochem Cytochem; 39(10), 1331-1336.

Walther FJ, Waring AJ, Hernandez-Juviel JM, Gordon LM, Wang Z, Jung CL, Ruchala P, Clark AP, Smith WM, Sharma S, Notter RH (2010). Critical structural and functional roles for the N-terminal insertion sequence in surfactant protein B analogs. PLoS One; 5, e8672.

Waring AJ, Walther FJ, Gordon LM, Hernandez-Juviel JM, Hong T, Sherman MA, Alonso C, Alig T, Braun A, Bacon D, Zasadzinski JA (2005). The role of charged amphipathic helices in the structure and function of surfactant protein B. J Pept Res; 66, 364-374.

Whitsett JA, Nogee LM, Weaver TE, Horowitz AD (1995). Human surfactant protein B: structure, function, regulation, and genetic disease. Physiol Rev; 75,749-757.

Wiedemann HP, Tai DY (1997). Adult respiratory distress syndrome (ARDS): current management, future directions. Clev Clin J Med; 64(7), 365-372.

William MC (1977). Conversion of lamellar body membranes in to tubular myelin in alveoli of fetal rats lungs. J Cell Biol; 72, 260-277.

Williams MC, Hawgood S, Hamilton RL (1991). Changes in lipid structure produced by surfactant proteins SP-A, SP-B, and SP-C. Am J Respir Cell Mol; 5(1), 41-50.

Wright JR and Clements JA (1989). Lung surfactant turnovers and factors that affect turnover. In: Massaro D, ed. Lung Cell Biology, New York, Marcel Dekker Inc; 655-699.

Yang TC, McDonald M, Morrow MR, Booth V (2009). The effect of a C-terminal peptide of surfactant protein B (SP-B) on oriented lipid bilayers, characterized by solid-state 2H- and 31P-NMR. Biophy J; 96, 3762-3771.

Yeagle PL (1996). Membranes: Phosphorus-31 NMR. In: Encyclopedia of Nuclear Magnetic Resonance. D.M. Grant and R.K. Harris, eds.John Wiley, Toronto, Canada; 3015-3022.

Zuo YY, Veldhuizen RA, Neumann AW, Petersen NO, Possmayer F (2008). Current perspectives in pulmonary surfactant-inhibition, enhancement and evaluation. Biochim Biophys Acta; 1778(10), 1947-1977.